



UNITED NATIONS  
UNIVERSITY

**UNU-GTP**

Geothermal Training Programme

Orkustofnun, Grensasvegur 9,  
IS-108 Reykjavik, Iceland

Reports 2015  
Number 26

## **BOREHOLE GEOLOGY AND HYDROTHERMAL ALTERATION MINERALOGY OF WELL MW-19A, MENENGAI GEOTHERMAL FIELD, KENYA**

**Fredrick M. Mutua**

Geothermal Development Company – GDC

P.O Box 17700-20100

Nakuru

KENYA

*fmutua@gdc.co.ke / fredmachokaa@gmail.com*

### **ABSTRACT**

Well MW-19A in Menengai is a directional well drilled to the north at an azimuth of  $339.92^\circ$  and inclination of  $20.19^\circ$  to a measured depth (MD) of 2355 m. The aim of drilling this well was to tap steam from NNW-SSE trending structures associated with the Molo Tectono-Volcanic Axis (TVA) and also to confirm the extent of the resource to the north inside the Menengai caldera. Comprehensive binocular and petrographic analyses of cuttings from the well indicate that the lithology of the well comprises five rock units i.e. pyroclastics, tuffs, trachytes and intrusions of syenitic and basaltic composition. Trachyte forms the main reservoir rock and it is the dominant rock below 504 m. These rock units host secondary hydrothermal mineral assemblages which are dependent on temperature, permeability, rock type and the chemistry of the circulating fluid. Hydrothermal alteration patterns show prograde alteration with increase in temperature and depth, as observed from alteration minerals in veins and vesicles. Five alteration zones were identified: unaltered zone (0-120 m), zeolite zone (120-502 m), chlorite-smectite zone (502-1100 m), quartz-illite-epidote zone (1100-1358 m) and quartz-illite-epidote-wollastonite-actinolite zone (1358-2355). Appearance of epidote at 1202-1760 m and actinolite at 1358-1882 m indicates that alteration temperatures have reached  $230^\circ\text{C}$  and  $290^\circ\text{C}$  respectively at these depths. Correlation of fluid inclusion analyses, alteration and formation temperature indicates two geothermal episodes; one of a high temperature geothermal system below 600 m depth and a recent second phase of cooling between 1140 and 1400 m. The well is also very permeable as observed from the intensity of alteration, oxidation, veining, in addition to circulation losses and the abundance of calcite and pyrite. Eight permeable locations were identified which were further grouped into four major aquifers deduced from temperature logs, and their locations correlate with the cutting data. The major feed zone below 1400 m is considered the dominant one in the well. Alteration mineral correlation of MW-19A with neighbouring wells of MW-22 and MW-11 suggests that the well is nearer to an up flow zone than the latter wells while the stratigraphic correlation between the wells reveals the existence of normal faults between MW-19A / MW-22 and MW-22 / MW-11.

## 1. INTRODUCTION

### 1.1 General information

Menengai is a high-temperature geothermal field situated north of Lake Nakuru and south of Lake Bogoria on the floor of the central Kenyan Rift (Figure 1). It encompasses the Menengai volcano, the Ol'Rongai volcanoes, Ol'Banita plains and parts of the Solai graben to the northeast. It is located at the triple junction between the main Kenya rift and the less prominent Nyanza rift. Deep geothermal wells have been drilled in the Menengai caldera and proved the existence of a geothermal resource. Currently, 28 deep wells of depths varying from 2,100 to 3,200 m have been drilled. Well MW-19A is the fourth directional well to be drilled in the Menengai geothermal field. The well is located at the dome area on the floor of the caldera and shares the same well pad with production well MW-19. It is defined by the UTM coordinates E 172629.35, N 9977723.82 at an elevation of 2072 m a.s.l. The well was aimed at tapping from the NNW-SSE trending structures associated with the Molo TVA. The specific objectives for drilling the well were to increase steam production for the planned 105 MWe Menengai power plant and establish the resource extent to the NW as well as providing additional information on sub-surface geology, hydrothermal alteration, and the chemical characteristics of the reservoir. The well was drilled to a depth of 2354 m from 16<sup>th</sup> October, 2014, to 6<sup>th</sup> January, 2015, i.e. for 87 days.

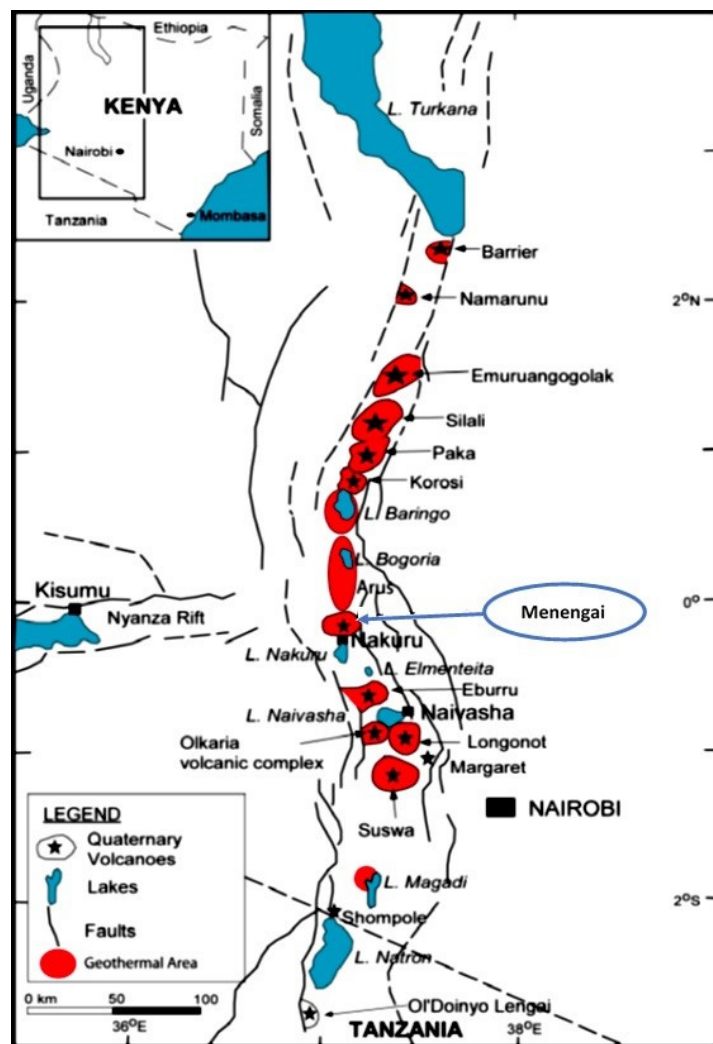


FIGURE 1: Location of the Menengai field within the Kenyan Rift Valley (modified from GDC, 2010)

### 1.2 Purpose of the project

The aim of this project is to study the borehole geology of MW-19A by analysing drill cutting samples taken in the well at 2 m intervals in order to identify the sub-surface lithology, determine the alteration and hydrothermal mineralogy, locate aquifers/feed zones, and try to conceptualize the geothermal system(s) and temperatures in the Menengai field.

### 1.3 Previous work

Menengai geothermal field has previously been studied by various geoscientists for various purposes/objectives including academically based research, regional geological mapping for government institutions and regional mapping with interests in natural resources, including geothermal. McCall was the first geologist to describe the Menengai volcano and the surrounding area. In his reports

(McCall, 1957a, 1957b, 1964, 1967) he provides a comprehensive account of many aspects of the geology of the area. Jones and Lippard (1979), Jones (1985), Griffith (1980), and Griffith and Gibson (1980) published reports on the geology of Menengai and the surrounding areas. Leat (1983, 1984) studied the structural and geochemical evolution of Menengai Caldera. In his reports, he described the volcano as being solely composed of peralkaline and silica oversaturated rocks.

Geotermica Italiana (1987) was the first group to carry out research focused solely on the assessment of the geothermal potential of Menengai. The project was coordinated and financed by UNDP and the Government of Kenya. It resulted in a detailed geological description of the area.

Another detailed geoscientific survey was conducted by KenGen and the Kenyan Ministry of Energy in 2004. The study involved geological, geophysical and geochemical surveys. The results from this survey indicated the existence of a hot, ductile, and dense body centred beneath the Menengai caldera. The study estimated that the high-temperature part of the resource covers an area of about 48 km<sup>2</sup> (KenGen, 2004).

In 2010, GDC conducted a comprehensive study in the Menengai prospect to confirm all geological observations recorded in previous work that might be associated with development and occurrences of a geothermal resource. Findings from this study point to the existence of exploitable geothermal resources within the Menengai caldera, Ol-Rongai and Ol-Banita calderas to the northwest of the Menengai caldera (Figure 2). This is evidenced by active strong surface manifestations and young lavas, signifying an active heat source. From this study, MT resistivity distribution at 2000 m b.s.l. shows a conductive body of less than 5 ohm-m under the caldera floor with a westward extension. Seismology indicates seismic wave attenuation at <6 km depth underneath Menengai caldera and Ol'rongai, suggesting the occurrence of shallow magma bodies which would be the heat sources for the geothermal system. (Simiyu and Keller, 1997).

Previous studies have led to the development of a geothermal conceptual model (currently being developed) with a hot magmatic body beneath the caldera floor with an up-flow under the caldera and an outflow to the north (Figure 2). In addition, gas geothermometry, based on H<sub>2</sub>S and CO<sub>2</sub>, indicates that the reservoir temperatures are greater than 250°C. Following these encouraging results, three exploratory wells were sited and a decision to commence drilling was reached.

Exploration drilling commenced in February 2011 and currently production drilling is underway and a total of 28 deep wells of depths varying from 2,100 m to 3,200 m have been drilled. Reservoir temperatures of up to 400°C at 2,000 m have been encountered in several wells making it the hottest geothermal system in Kenya. Steam production from the wells varies from small to greater than 10 MWe.

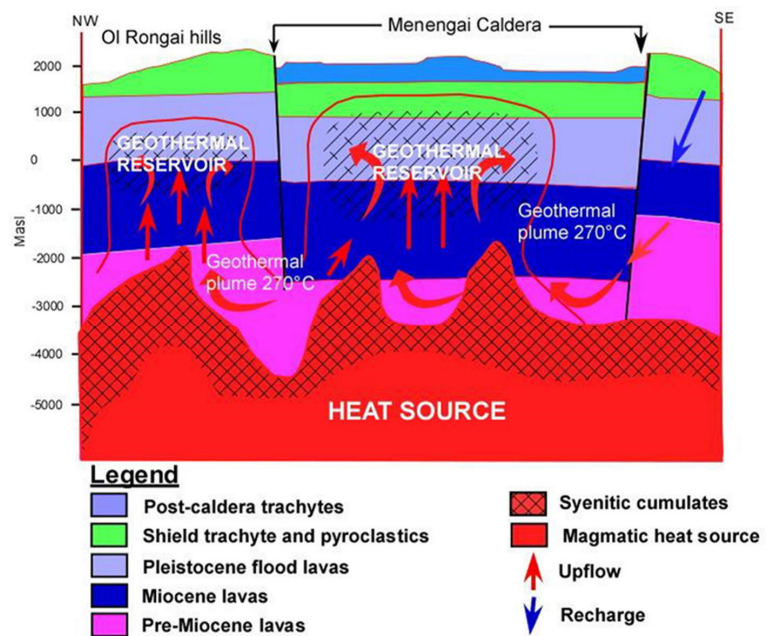


FIGURE 2: Menengai geothermal model (GDC, 2010)

Borehole geological studies on completed wells (Omondi, 2011, Mibei, 2012; Kipchumba, 2013; Lopeyok, 2013; Mbia, 2014; Kahiga, 2014) have also been done to further re-evaluate the geothermal system. Further structural mapping has recently been carried out (Strecker et.al, 2013), with the aim of studying the young structural evolution of the greater Menengai area north of Nakuru in light of the ongoing geothermal exploration and structural assessment of this sector of the central Kenya Rift.

Currently 132.5 MW of steam equivalent is on the wellheads and full steam production for the planned 105 MWe power plants is expected before the end of 2015 (GDC, 2015). Three Independent Power Producers (IPPs) have been licensed for 20 years to operate 35 MWe modular plants each. In addition, GDC has recently successfully piloted four projects on the direct utilization of steam in a move aimed at diversifying geothermal use apart from power generation in Menengai. These are: geothermal powered dairy unit, geothermal powered laundry, geothermal heated aquaculture ponds and geothermal heated green houses.

## **2. GEOLOGY AND STRUCTURAL SETTING**

### **2.1 Regional geology**

The East African Rift is an active continental rift zone in eastern Africa that appears to be a developing divergent tectonic plate boundary where rift tectonism is accompanied by intense volcanism. The rift is a narrow zone in which the African plate is in the process of splitting into two new tectonic plates (McCall, 1967). It runs from the Afar Triple Junction in the Afar depression southward through eastern Africa. The East African Rift System consists of two main branches; the Eastern Rift Valley and the Western Rift Valley. These resulted from the actions of numerous normal (dip-slip) faults which are typical of all tectonic rift zones (Strecker et al., 1990).

The Kenya Rift Valley comprises 14 geothermal prospects (Figure 1) starting from Barrier in the north to Lake Magadi in the south (Omenda, 2000). It forms a classic graben with an average width of 40-80 km, dotted by several Tertiary volcanoes. The rift floor is comprised mainly of the eruptive materials from these volcanoes (McCall, 1957). Most of the volcanic centres have gone through one or more explosive phases including a caldera collapse. Some centres are dotted with hydrothermal activity and are envisaged to host extensive geothermal systems which are driven by hot magma at shallow depths in the crust (Dunkley et al., 1993, Suwai, 2011).

The Menengai geothermal prospect is located within an area characterized by complex tectonic activity associated with a rift triple junction. This is a zone at which the failed rift arm of the Nyanza rift joins the main Kenyan rift. The Kenyan rift is characterized by extensional tectonism where the E-W tensional forces resulted in block faulting, which includes tilted blocks as evident in both the floor and scarps of the rift (KenGen, 2004). Narrow scarps that show little effect of movement have been eroded resulting in gentle scarps characterize the western margin. The eastern margins, however, depict wider belts with sharp scarps, implying recent active movements. The rift trough is cut by numerous normal faults that clearly represent continued extensive tectonism under the rift floor (Gichira, 2012; KenGen, 2004).

### **2.2 Geology of Menengai volcano**

The Menengai geothermal field region comprises Menengai volcano, the Ol'rongai volcanoes, the Olbanita plains, and parts of the Solai TVA to the northeast (GDC, 2010) covering an area of approximately 950 km<sup>2</sup> (Figures 3 and 4). Menengai is one of the Quaternary volcanoes formed on the axis of the Kenyan Rift (Figure 1). It is a trachytic central volcano that is underlain by a shallow magma chamber. The activity in the volcano started 0.2 Ma ago with the formation of a broad low angle trachytic

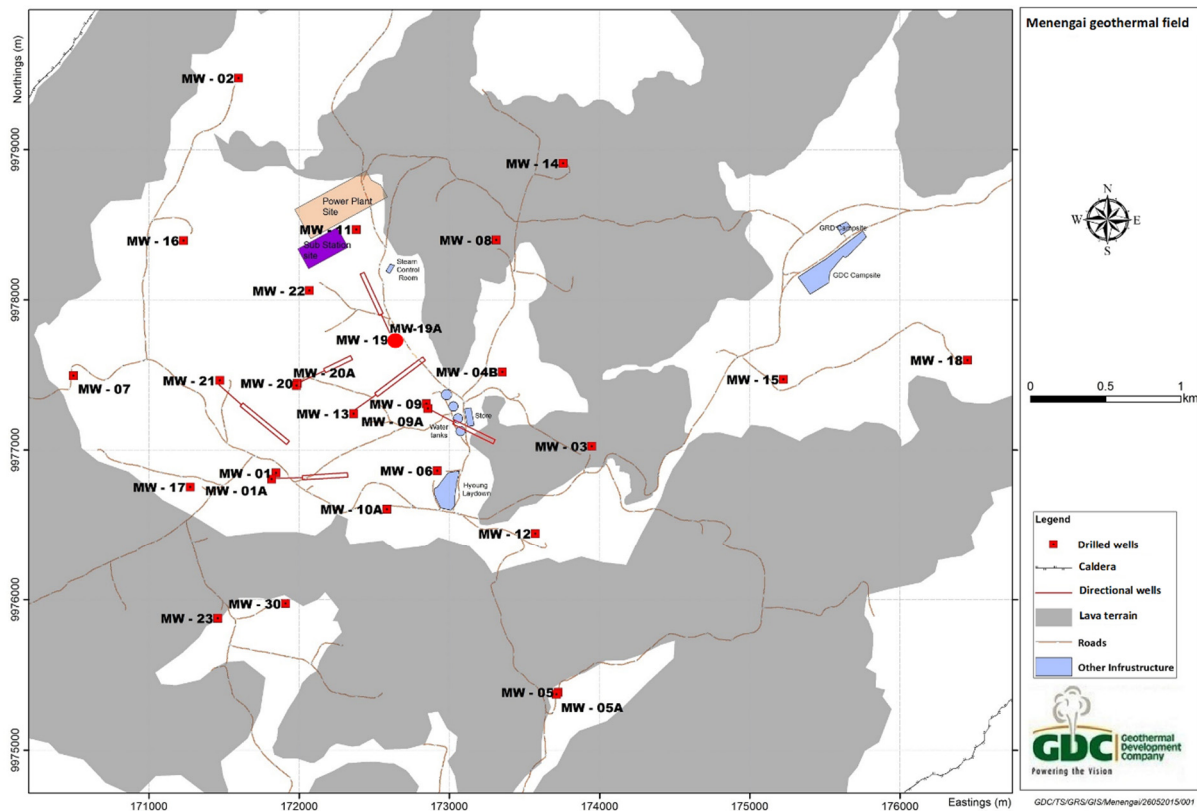


FIGURE 3: Location of well MW-19A, highlighted in a red circle (GDC, 2015)

lava shield (Leat, 1984). The activity continued in the Pleistocene, with the formation of a caldera, to more recent activity that has given rise to the flows on the caldera floor (Macdonald et al., 1970).

The surface geology is dominated by recent (post caldera) lavas, especially within the caldera, pyroclastics and ignimbrite sheets on the northern flanks and alluvial sediments on the surrounding rift floor (Figures 3 and 4). The geology and evolution of the Menengai caldera is intricately tied to the volcanology of the Kenyan Central Rift Valley and can be divided into three main phases: pre-caldera volcanics, syn-caldera activity, and post-caldera activity.

The first phase, the pre-caldera phase, is associated with the

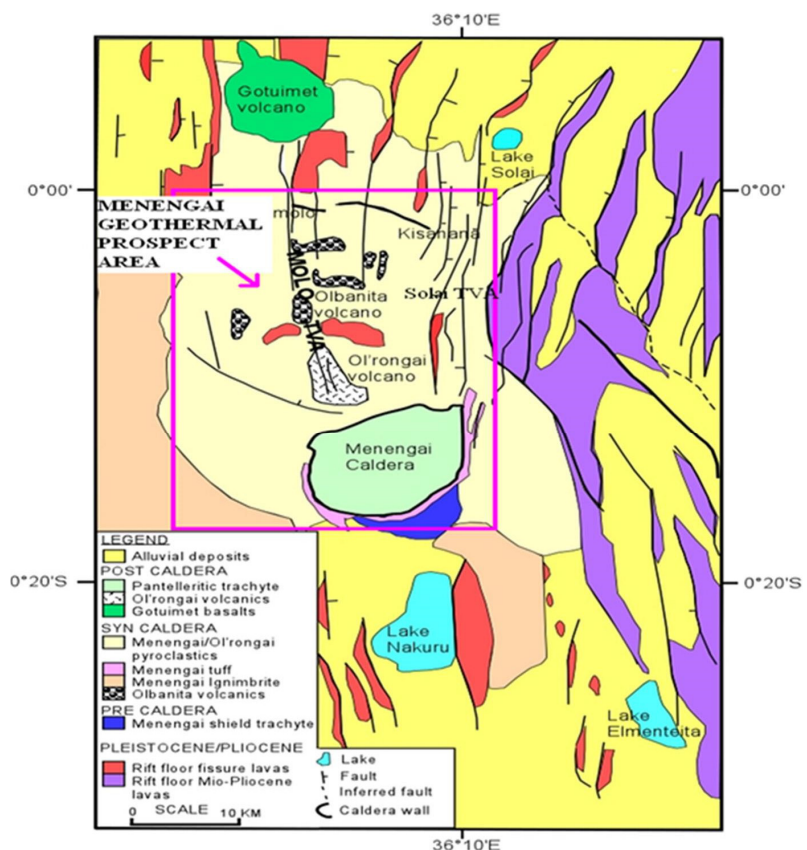


FIGURE 4: Simplified geological map and extent of the Menengai field (GDC, 2010)

formation of the shield and the eruption of lavas that preceded the collapse of the caldera. Pre-caldera volcanics now form low hills which slope away from the rim of the caldera. The rocks formed during this period are not visible on the caldera floor owing to mantling by thick syn- and post-caldera volcanics. There are, however, good exposures of these rocks at the caldera wall, especially at the Lions Head cliff (view point). The only other outcrop away from the caldera wall is the ballast quarry off the Nakuru-Bahati road. The height of the caldera wall, and thus the exposed thickness of the volcanics, varies dramatically around the caldera. The total throw of the caldera wall at the Lion's Head Cliff is about 300 m, where almost the entire 235 m pre-caldera succession is composed of simple trachyte lavas, most of which are dark grey and slightly fissile. The mean thickness of the flows is 23 m, varying between 11 m and 60 m. Tops of lavas are blocky, transitional to a crude, vesicular pahoehoe; no well-developed roopy tops are seen. Air-fall pumice deposits make up only about 1% of the thickness of the Lions Head section, and there are no pre-caldera ash flows. Almost constant thickness of reddened soil horizons separating many lavas suggests that eruptions took place at regular intervals. These lavas are all trachytic with the groundmass being composed of mainly sanidine crystallites. Some riebeckite/arfvedsonite are also present. Large (up to a meter) to small lithic inclusion of syenitic rocks are common. The pre-caldera lavas have been dated at  $0.18 \pm 0.01$  My (Leat, 1983) and, therefore, the shield volcano is estimated to be around this age.

The second phase, the syn-caldera activity, is associated with the caldera collapse. The incremental caldera collapse is believed to have occurred in two episodes (Leat, 1984; Macdonald and Scaillet, 2006). The formation of the  $11.5 \times 7.5$  km large caldera was accompanied by the eruption of two ash flow tuffs. Each of the tuff layers is underlain by a pumice deposit and separated by a thin layer of sediments, indicating a short quiescence period between the eruptions (Leat, 1984). The collapse is mainly associated with the second ash flow eruption. The syn-caldera rocks are spread around the Menengai caldera and comprise ignimbrite and pumice/ash deposits. They are exposed both at the upper parts of the caldera rim (east and northern rim), where the rim resembles an agglomerate deposit, which is rich in poorly sorted angular lithic and glassy/semi-pumiceous material. The syn-caldera rocks show flow texture (rheomorphic) indicative of a pyroclastics flow mode of emplacement. This is the proximal phase indicating that the source was at the caldera and its rim. Other exposures away from the caldera rim include extensive mantling of the ground in the north and west (Kampi Ya Moto, El Bonwala and Ol'rongai areas) where there is a slight transition due to distance of transportation before deposition occurred. Here the ignimbrite resembles welded tuff with numerous collapsed pumice fiamme depicting eutaxitic texture'. This is a distal facies of deposition. Further away to the north and east, this formation is thin (few centimetres to meters) and occurs as ash tuff, representing the distal facies. The age of the syn-caldera pyroclastics has been published by many researchers, e.g. Leat (1983) published an age of  $29,000 \pm 300$  years for the older eruptives and 12,850 years for the younger ones. Geotermica italiana Srl (1987) published an age of  $14,900 \pm 900$  years based on carbon dating of palaeosoils between the syn-caldera eruptives.

The third phase, the post-caldera activity, mainly involved eruptions of recent lavas and ash deposits from vents within the caldera. This eruption episode probably occurred contemporaneously both inside the caldera floor and at Ol'rongai. Several distinct lava flows can be identified on the caldera floor, with most of the eruption centres emitting the flows located in the central and western parts. These lavas have built a huge pile inside the caldera rising to 2160 m a.s.l. and estimated to be about 300 m thick. The lowest part of the caldera floor, which is also in-filled with the same lavas, stands about 1700 m a.s.l.

During the post-caldera era, lava and ash eruptions continued with most of the activity being concentrated within the caldera summit. Several vents and eruption centres like "Mlima punda" can be identified within the summit area. Mlima punda is one of the cinder cones formed by an explosive eruption emitting scoria due to the high amounts of volatiles in the magma. Generally, all rock formations and cinder cone structures seen on the caldera floor are of the post-caldera stage. The lavas are dark in colour, holocrystalline, glassy and vesicular (Mibei 2012).

The ropy flow texture, which is still intact, indicates a young age and the low viscosity of the lavas. Samples from the thicker part (non-vesicular) show that they are trachytes with the groundmass exhibiting a strong trachytic flow texture. The groundmass is mainly made up of sanidine feldspar laths and occasional riebeckite crystallites. An age of 1,400 yrs for the post-caldera lava is published by Jones and Lippard (1979). The apparent lack of disturbance in the thin flow tubes in the ropy texture indicates that some of these lava flows are younger than the specified age (Leat, 1984).

Other post-caldera lithological units are the lake sediments in the northeast near the gate barrier. This formation is evidence of a palaeo intra-caldera lake presumed to be from 8,000-10,000 yrs. BP as proposed by Leat (1984) and could have formed minor components of the recharge to the Menengai geothermal system. The lake was formed as a result of subterranean outflow of Lake Nakuru through structures and faults associated with the Solai system. The diatomaceous deposits associated with this Palaeo-lake are overlain by post-caldera volcanics.

### 2.3 Structural geology

Menengai Geothermal field is located within an area characterized by complex tectonic activity associated with the rift triple junction. This is a zone at which the Nyanza half-graben (failed rift) joins the main Kenyan rift (KenGen 2004, Burke and Dewey, 1973). The floor of the Menengai caldera depicts extensional tectonics with the main trough trending N-S north of Menengai and NNW-SSE south of Menengai. Menengai is therefore set at a point where the Kenyan Rift abruptly takes a sharp change in direction. This change is associated with the contact between the Tanzanian craton and orogenic belts (Simiyu and Keller, 1997). The floor of the Menengai area depicts extensional tectonics with spatial variation in the stress regime, indicated by different styles in the orientation of faults north of the caldera. The structures associated with Ol'rongai system are oriented to the NW-SE and are related to the NW-SE Menengai pre-caldera shield orientation (Figure 5) (Leat, 1984). On the other hand, faults associated with the Solai system have a NE-SW orientation, also assumed by the Menengai caldera. Therefore, the faults appear to have influenced the caldera's formation. Most structures in the Solai system can be extrapolated and cut into the caldera rim, indicating that some of these faults are in fact younger than the caldera. The variation in the orientation styles of the old NW-SE structures and the younger NE-SW structures could be due to a change or a shift in the crustal stresses. Generally, the main structures in the Menengai field (Figure 6) can be divided into three main groups, namely:

- a. The Menengai caldera and ring faults;
- b. Ol'rongai and the Molo Tectono-volcanic axis TVA;
- c. The Solai structural system.

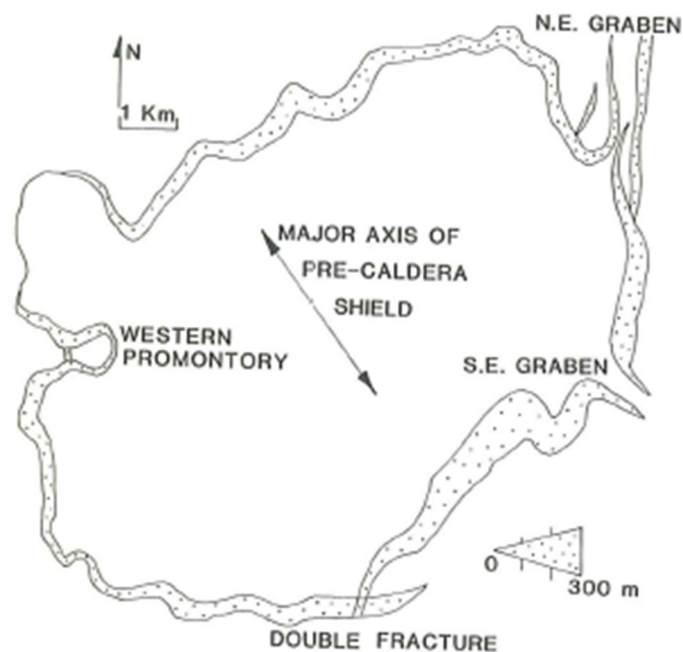


FIGURE 5: Topography of Menengai caldera (Leat, 1984)

### 2.3.1 The Menengai caldera and ring faults

The Menengai caldera is an elliptical depression with minor and major axes measuring about 11.5 km and 7.5 km, respectively (GDC, 2010). The circular rim of the caldera ring fault is well preserved with vertical cliffs at some places measuring up to about 400 m. The ring structure has been disturbed only by the Solai graben faults on the northeast end and another fracture at the south-southwest end of the caldera wall extending southwards (Figure 6).

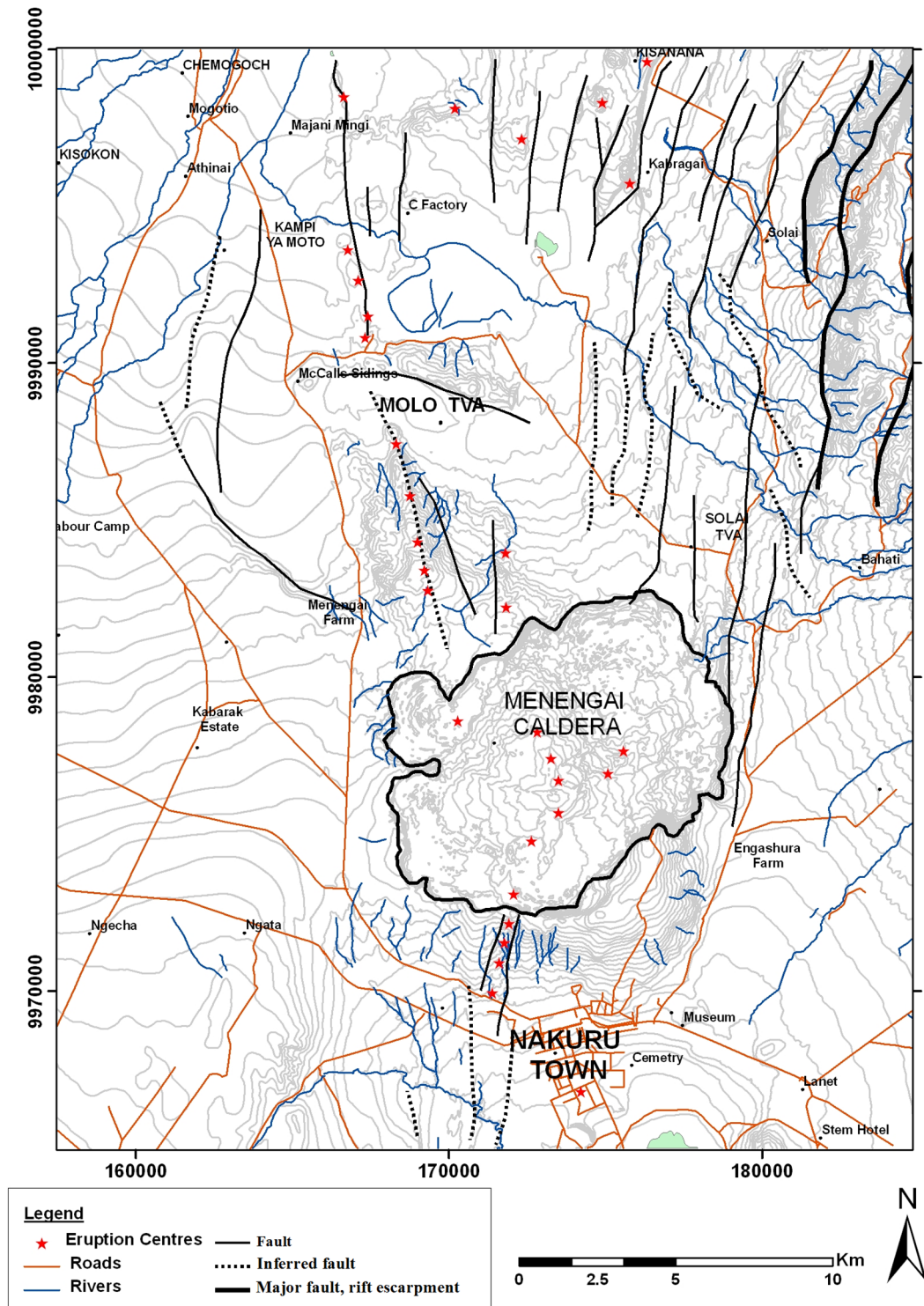


FIGURE 6: The main geological structures in the Menengai geothermal field (GDC, 2010)



Other disturbances at the southeast and northwest ends may be grabens that existed before the caldera collapse. Two large fragments of caldera wall have remained in a partially collapsed condition since the caldera formation (McCall 1957a, 1967, Leat, 1984). The most striking feature is the Western promontory which location can be seen in Figure 5. This block dropped only 60 m and was tilted 8° to the S during the collapse. Some minor (1 m) post caldera movements have taken place on the fault which separates the Promontory from the main part of the caldera wall. This movement disturbed early post caldera tephra beds and dropped the Promontory further into the caldera. The other partial collapse feature, the Double Fracture (Figure 5) consists of a tilted block.

Leat (1984), described the presence of the fault-bounded sector graben and the partially collapsed features suggest that the portions of the adjacent caldera wall also represents surface expressions of faults, and the embayment's in the caldera wall are not the back-walls of landslips but are the surface expressions of an embayed ring fracture. Also, some post caldera vents occur close to the caldera wall, perhaps marking the position of a major fault. The presence of embayment's in the ring fracture and the partial collapse features suggest that the cauldron block foundered as dislocated pieces, not as a simple piston. The random arrangement of some post-caldera vents is further evidence that the cauldron block is fractured. The caldera floor is covered with post-caldera lavas such that tectonic structures are hardly seen. However, most of the caldera infill lavas are fissure eruptions that billowed out of the fracture openings (Leat, 1984). Mibei (2012) suggests that most structures can be extrapolated into the caldera, based on evidence in and around the caldera walls as well as using the flow direction of lavas and hotspots mapped by infrared spectroscopy by Schwonke, (2009). At the central part of the caldera, a fissure with a NW-SE orientation has been mapped; this fissure may have resulted from transform faulting. A portion of the post-caldera lavas appears to have erupted from this fissure in a sub-plinian style. Strecker and Melnick (2013), mapped numerous linear features oriented either ESE-WNW or E-W, in the central area of the Menengai caldera. They attributed this to the central doming which is associated with magma intrusions. Additionally, these features are characterized by numerous fractures with aligned fumaroles, some of which are active and sulphurous.

### **2.3.2 The Molo Tectono-volcanic axis (TVA)/ Ol'rongai structural system**

The Molo Tectono-volcanic axis (Geotermica Italiana, 1987) is a very prominent volcanic feature represented on the surface by a zone with a concentration of faults and fractures with a NW-SE orientation and along which volcanic eruptions have taken place (Figure 6) that resulted in the formation of a NNW trending ridge, referred to as the Ol'rongai volcano.

On a regional scale, the Ol'rongai system extends northwards through Lomolo to as far as Gotuimet volcanic centre (Figure 6). Over the Ol'rongai area, the structure is marked by intense volcanic activity including explosive (pumice issuing) craters. This part of the structure is adjacent to the Menengai caldera and possibly extends into the caldera. Although obscure on the surface, the structure probably extends into the Menengai caldera system and beyond, giving rise to the Makalia fault system, which pass through the western part of Nakuru Town. The apparent intense volcanism indicated by numerous eruption centres in the western part of the Menengai caldera is probably due to the intersection of the caldera structures and the Molo TVA/ Ol'rongai fracture system (KenGen 2004). Leat (1984) argued that the Menengai pre-caldera shield had the same orientation as the described NW-SE structures and was probably influenced by these faults.

### **2.3.3 The Solai structural system**

The Solai structural system, referred to as the Solai graben (4 km on average), includes structures that run in a N-S direction from the eastern end of Menengai caldera, through Solai (Figure 6). It is comprised of numerous faults/fractures all trending in a N-S direction. The eastern boundary of the graben probably extends to the foot of Marmanet escarpment. This is the only system that has cut the Menengai pyroclastics. On the northern end, it also cuts through the Pleistocene trachyphonolites of the Lake Bogoria suite NW of Kisanana out of the Menengai field. Its southern extension under the Menengai

volcanic pile is an important hydrogeological control and a possible permeability enhancement of brittle lava formations underlying the Menengai eruptives (KenGen, 2004).

## 2.4 Hydrogeology and surface drainage systems

The surface drainage system is largely from the east and the western scarps. On the rift floor, the drainage is mainly from Menengai caldera northwards with the exception of the drainage from the southern rim, or slopes of Menengai caldera, into Lake Nakuru (Kuria and Woldai, 2003). The N-S, NE-SW, and NW-SE trending fault/fracture systems provide underground channels resulting in stream water disappearing underground (Suwai, 2011). The hydrogeology of the area is mainly inferred from data obtained from water boreholes. Information on aquifer properties and groundwater flow patterns is provided by interpretation of data from these boreholes, the majority of which were drilled to 100-200 m depth. However, on the caldera floor, greater reliance is placed on indirect methods of assessing recharge, e.g. surface hydrological information due to a paucity of borehole data. The relative yields of the boreholes may be matched with the petro-physical properties of the feeder formations, which range from dry and thermally anomalous boreholes to very high yield boreholes ( $>20 \text{ m}^3/\text{h}$ ). The dry and elevated temperature boreholes are distributed along the Molo TVA that extends from the Menengai caldera northward through the Ol'Rongai volcano, Lomolo and Gotuimet volcano. The high yield boreholes are located to the east of the caldera and are bound by the Bahati and Marmanent scarps which are relatively wetter and on higher grounds. Earlier studies have shown that these areas are fed by channels along the rift scarp faults (Kipng'ok, 2011).

## 3. SAMPLING AND ANALYTICAL METHODS

### 3.1 Sampling

Samples for this project were obtained from well MW-19A in the Menengai geothermal field. Drill cuttings were sampled at a 2 m interval during drilling after which preliminary analysis was performed at the rig site through binocular microscopy. No cores were recovered from this well and therefore, all the descriptions and interpretations are solely based on cutting samples. The main objective was to identify the lithology, alteration minerals, feed zones and possible foreign materials in the cuttings, such as bit fragments. The aim was to develop a preliminary lithostratigraphy and estimate the down-hole temperatures based on alteration mineralogy. This helped in the determination of casing depths and also to foresee possible imminent problems that might occur during drilling operations due to geological factors. The samples were then processed further by washing and drying in preparation for thin-section and XRD analyses. In the present study, however, a more detailed analyses of the samples from well MW-19A were carried out at the ISOR (Iceland GeoSurvey) geological laboratories.

### 3.2 Analytical methods

With the aim of characterizing the borehole geology and the hydrothermal alteration mineralogy of well MW-19A, several analytical methods were employed in this study. These include; binocular microscope analysis, petrographic microscope analysis, X-ray Diffractometer analysis (XRD) and fluid inclusion analysis. A brief description of these analytical techniques is provided below:

#### 3.2.1 Binocular microscope analysis

Samples were analysed at a 2 m interval using a binocular microscope. The samples were carefully washed with clean water to remove impurities and dust to enhance visibility of samples and obscure features such as finely disseminated sulphides e.g. pyrite and chalcopyrite. The aim of this analysis was to identify the lithology, texture, alteration mineralogy, degree of alteration, fracturing and probable aquifers. The samples were analysed using an *Olympus SZX12* binocular microscope and the properties

noted include: the colour of the rock, grain size, texture, vein filling if present, alteration mineralogy, and degree of alteration; from these observations, the rock types and their properties were identified. Dilute HCl was used to identify the presence of calcite; caution was taken at depths where foreign material from cement plugging or cementing of casing was suspected. Samples of interest were selected for XRD analysis. In addition, calcite and quartz grains from different depths in MW-19A were picked for fluid inclusion geothermometry analysis.

### 3.2.2 Petrographic microscope analysis

Based on preliminary binocular analysis performed at the rig site, representative samples from different depths and lithologic units from MW-19A were selected for petrographic analysis. A total of 26 thin sections were prepared at the GDC laboratory. The thin sections were analysed using a Leitz Wetzler petrographic microscope at ISOR, Icelandic GeoSurvey laboratories. The purpose for this analysis was to confirm the rock types and the hydrothermal alteration minerals and any other additional minerals that were not observed under the binocular microscope. The analysis also aimed at identifying the paragenetic sequence and patterns of the alteration minerals in veins and vesicle fillings.

### 3.2.3 X-ray diffractometer analysis

This technique is mainly used for the identification of clay minerals and zeolites. Clay minerals are known to have diverse mineralogy and crystal structures, thus, are not easily distinguishable by microscopic analysis. A total of 18 samples were selected and prepared for XRD analysis. Here, untreated, glycolated and heated samples were run. The main aim of the analysis was to identify clay alteration mineralogy with depth and further deduce the temperature regime in the system.

Small portions of cuttings from selected samples were scooped and mixed with water in test tubes. The mixtures were shaken for 4-5 hours to dissolve and extract clay from the cuttings. A few drops of water from each of the dissolved drill cutting samples were placed on separate glass slides which had been washed previously with an organic solvent, acetone, and dipped in a glycol solution for 24 hours. The samples in the test tubes were left to settle for 12 hours. The clay samples were first run in the X-ray diffractometer (Bruker AXS, D8 Focus Diffractometer) and the peaks recorded. The glycolated samples were subsequently run in the X-ray diffractometer and the peaks were recorded. The clay samples were heated to 550°C before performing the third run in the X-ray diffractometer and the peaks were recorded. For each sample, three peaks, each from the corresponding runs, were recorded. Results of the XRD analysis for MW-19A are summarized in a Table 2 while some graphical presentations of some results are displayed in Appendix I.

### 3.2.4 Fluid inclusion analysis

Fluid inclusion analysis is the study of fluids trapped in vacuoles inside mineral grains during growth or recrystallization. The trapped fluids, termed as fluid inclusions, give an approximate temperature from the time when the fluid was trapped in the mineral grain. This is measured by heating the crystal until the fluid inclusion reaches the homogenization temperature ( $T_h$ ). In this study, calcite and quartz grains from different depths in the well were hand-picked for fluid inclusion geothermometry analysis. Since the crystals were not clear enough, they were polished to enhance their transparency. Upon confirmation by use of the petrographic microscope of the presence of clear fluid inclusions, the grains were slowly heated, each at a time, on a Linkam THSMG 94 heating and freezing stage until the fluid homogenized in a single phase (i.e. bubbles disappeared) and the temperature of homogenization ( $T_h$ ) was measured. Fluid inclusion geothermometry, when compared with results from alteration mineralogy and measured temperatures from the well, provide important information on the thermal history of the geothermal system. It provides evidence as to whether a geothermal system is heating up, cooling or is in equilibrium. The data acquired from all of the above analyses was intergrated using LogPlot 7 from RockWare Inc., a software which is very useful in correlating and interpreting geological and geotechnical data.

## 4. BOREHOLE GEOLOGY

### 4.1 Drilling of well MW-19A

Well MW-19A was spudded on 19<sup>th</sup> October, 2014 at 1715 hours and completed on 14<sup>th</sup> January, 2015 after which the rig was released for demobilization. It took 87 days to complete. MW19A is a directional well drilled to the north at an azimuth of 339.92° and inclination of 20.19° to a measured depth (MD) of 2355 m CT. The drilling was conducted in the following four main stages (Figure 7):

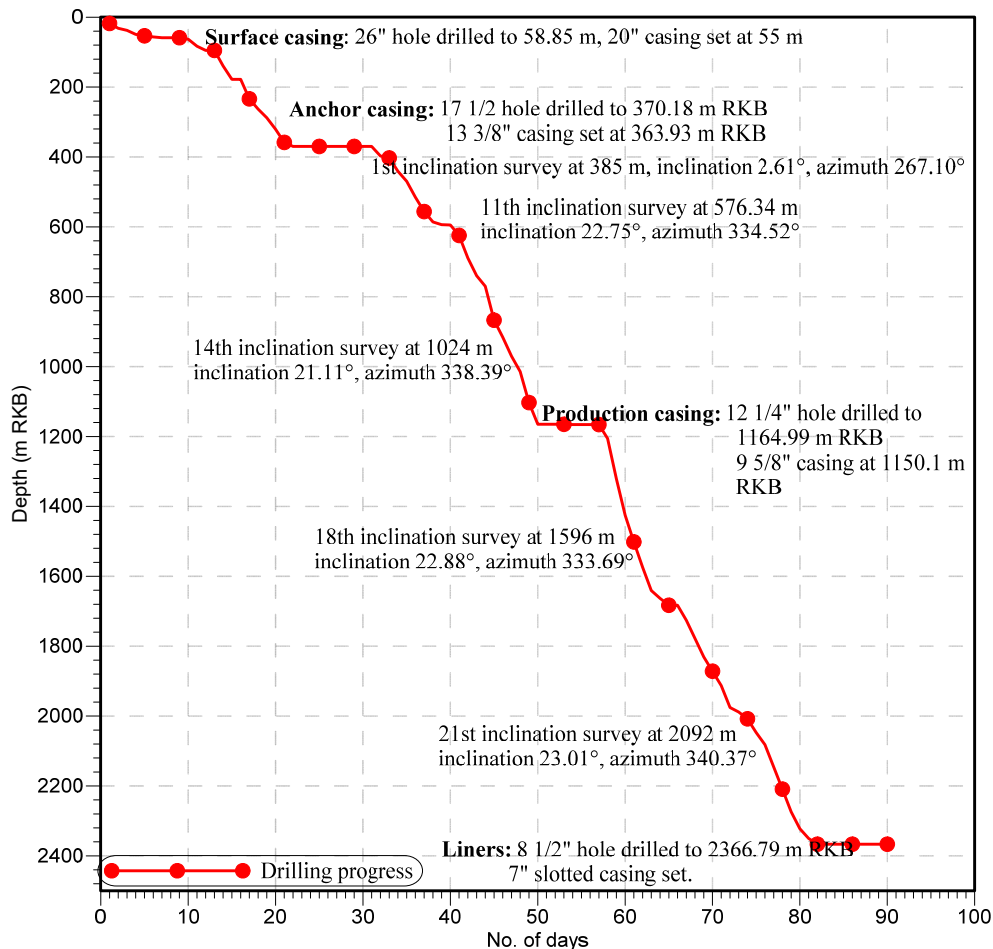


FIGURE 7: Well MW-19A drilling progress

*Stage one (drilling of 26" hole):* The 26" hole was drilled to a depth of 58.85 m with intermittent losses experienced. This section was drilled with water complemented by mud gel sweeps. The 20" casing was run in hole with the shoe set at 55 m. A total of 5 casing joints were run in where primary and secondary cementing was done. One backfill cement job was done in this section with a total of 19.02 tons of cement slurry being used to bond the 20" OD 94 lb/ft BTC casing.

*Stage two (drilling of 17½" hole):* The 17½" hole was drilled to a depth of 370.18 m with the 13⅜" casing being set at a depth of 363.93 m. A total of thirty-one 54.5 lb/ft casing joints were run in the hole. Three plug jobs and eleven backfill cement jobs were done in this section with a total mass of 333.32 tons of cement being used for both the casing and plugging jobs.

*Stage three (drilling of 12¼" hole):* The third drilling stage for the production casing was drilled with varied BHA. This is because the well was directional and it is at this section that the kick-off angle is built. To attain the kick-off angle, a rat hole at 400 m was drilled using slick BHA. POOH to change

from slick to kick off BHA followed. Drilling continued using aerated water and foam with returns being received on the surface. At 593.78 m the drill string was pulled out to change kick off BHA to lock up BHA and drilling of the 12¼" hole with aerated water and foam continued with partial returns received on the surface. Total loss of circulation was experienced at 902 m. Drilling blindly continued down to 970 m where POOH was done to change bit. After bit change, the hole was drilled with aerated water and foam with full returns received to casing depth of 1154 m CT. POOH to shoe to do wiper trip was done and 9⅝" casings run in. A total of 100 casings were run in. Casing shoe was set at a depth of 1150.1 m RKB. Primary cementing and three backfills were completed before returns were received on the surface. A volume of 109.81 tons of cement was consumed in this section for both casing and one plug job.

*Stage four (drilling of 8½" hole):* The 8½" hole section started on the 55<sup>th</sup> day of drilling with backing off of 9⅝" landing joint. Top of cement was tagged at 1116 m. Drilling out cement using slick BHA and water commenced with returns received on surface down to a depth of 1155 m. An integrity test of the shoe was done but the shoe failed. It was decided to cement plug. Mule shoe was placed 11m above the shoe and 1.3m<sup>3</sup>@ 1.8 g/cm<sup>3</sup> cement slurry pumped. After WOC, top of cement was tagged at 1139.94 m using mule shoe and slick BHA run in to DOC. DOC continued up-to 1165.15m where the slick BHA was pulled out of hole to change to pendulum BHA. An obstruction was tagged at 1124.98 m when running in the pendulum assembly and the hole was reamed. Drilling in formation using aerated water and foam with returns received on the surface continued to a depth of 1309.9 m where a gyro-survey was done. Drilling on bottom continued to a depth of 1663.2 m where POOH was done to change bit. On RIH with new bit, fill was tagged at 1650 m and the hole was reamed with aerated water and foam. Drilling then continued to a depth of 1683.10 m with 60% returns received on the surface. At this depth drilling was due to high torque and the hole reamed down from 1680 to 1683 m. Encountered consistent torque and fill at 1681m and decided to POOH to change BHA (remove SSTB2) and extract bit nozzles. After BHA change, drilling continued blindly to a depth of 1688.50 m where circulation was regained. Drilling on bottom with aerated water and foam continued to a depth of 1779.34 m with returns received on the surface. Circulation was done at this depth to clean hole after experiencing high torque before continuing to drill to a depth of 1988.32. POOH was then done to inspect the bit. It was discovered that the bit bearings were completely worn out. New bit was run in and drilling continued to a depth of 2081.80 m where TLC was experienced. Drilling blindly was then done from 2081.80 to 2146 m. From 2146 to 2322 m drilling was done using aerated water and foam with partial and intermittent returns received on the surface. TLC was experienced at this depth and blind drilling continued to TD of 2366.79 m. Wiper trip and POOH was done and 7" liners run in. This was followed by well completion test; the well was capped with a 10" class 900 master valve and completed on the 87th drilling day.

## 4.2 Stratigraphy

Based on both binocular stereo microscope observations and petrographic analysis five types of rock formations were found to form the litho-stratigraphy of MW-19A. These include: pyroclastics, tuff, trachyte, syenite and basalt. The lithology of the well is shown in Figure 8, in addition to alteration mineral distribution and alteration zonation.

### *Pyroclastics*

Pyroclastic fragments are found on the surface and occasionally as highly oxidized thin layers intercalating with trachyte lavas in Menengai. They form conspicuous thin lenses in the upper 450 m of the stratigraphy well column, signifying several pyroclastic eruptions in the post-caldera stage. The pyroclastics appear as brownish to grey, loose unconsolidated deposits composed of ash and vesicular fragments of pumice lapilli particles, obsidian, glass and lithics of trachytic composition. Oxides and some calcite are the main alteration minerals found in this formation however, zeolites and chalcedony are also found infilling vesicles.

### *Tuffs*

Tuffs were rare in this well and occur as thin intercalations at 368-372 m, 388-400 m, 492-504, and at 836-842 m. They are generally reddish brown to grey, commonly composed of non-welded, poorly crystalline and vitrified volcanic ash with vesicular texture. The tuffs were observed often altering to clays along contact boundaries. Four major tuff marker horizons were identified in MW-19A, which possibly demarcate the post, syn- and the pre-caldera volcanics. These markers are defined by tuffs encountered at 368-372 m, 388-400 m, 492-504 m and 836-842 m.

### *Trachyte*

Trachyte is the most dominant rock encountered in the well right from top to the bottom of the well where it occurs alternating with tuff, pyroclastics, basalt and syenite. The rock is light grey to dark grey in colour, fine grained and feldspar phyric composed of mainly feldspars, quartz, pyroxenes and mafic minerals. The rock has large feldspar phenocrysts (e.g. sanidine) surrounded by minute dark minerals, some exhibiting trachytic texture. Pyroxenes and minor amphiboles are the main mafic minerals present in this rock unit. The matrix consists of flow oriented feldspar microlites in a fine grained to glassy groundmass. The rock generally shows weak to moderate intensity of alteration except where the formation is fractured; when high intensity of alteration occurs the grey lava transforms either into a light greenish colour or appears bleached giving the rock a mottled texture.

In an endeavour to characterize different episodes of lava eruptions, trachyte in this study was classified into three groups based on its grain sizes; these are: fine-grained, medium-grained and coarse-grained trachytes. Although the chemistry of these rocks may vary slightly, textural classification was preferred.

### *Basalts*

First occurrence of basalt was at 1672-1674 m, and then at 1770-1802 m. The rock is dark grey to almost black in colour, with holocrystalline groundmass composed of plagioclase laths and anhedral clinopyroxenes and magnetite. It is porphyritic with phenocrysts of augite, plagioclase and olivine.

### *Syenite intrusions*

Menengai caldera is hosted in a spreading zone, hence, fresh magma pulses from the main magma chamber are readily injected into the overlying formations, forming dikes and other intrusions. These magma injections are facilitated by faults and fractures resulting from the tectonics associated with a divergent plate setting (Mibei, 2012). In MW-19A, syenite intrusions were encountered at 1418-1584 and 1920-1952 m depths. These intrusions are relatively fresh, grey coarse- to medium-grained, porphyritic with phenocrysts of feldspars, clinopyroxene (e.g. augite) and amphiboles. A summarized description of each of the lithologic units encountered in well MW-19A is given in Appendix II and plotted in Figure 8.

## **5. HYDROTHERMAL ALTERATION**

In well MW-19A, hydrothermal alteration minerals appear both as replacement of the primary minerals, as well as fillings in vesicles, vugs and fractures. The distribution and abundance of the hydrothermal minerals (Figure 8) were obtained from binocular, petrographic and XRD studies of drill cuttings samples taken after every 2 m from the well.

The distribution and abundance of any kind of mineral assemblages present in hydrothermal systems is influenced by several factors, which include, permeability, rock and water composition, temperature, pressure and duration of hydrothermal alteration (Browne and Ellis, 1970). These factors are largely independent, but the effects of one or more of the factors can exert a dominant influence on the location and extent of hydrothermal alteration. Permeability in rocks plays a crucial role in the access of thermal fluids, which cause hydrothermal alteration of the rocks and precipitation of secondary minerals in open spaces. Rocks, which possess very restricted permeability or are completely impervious to fluid, will only be slightly altered or show no alteration at all.

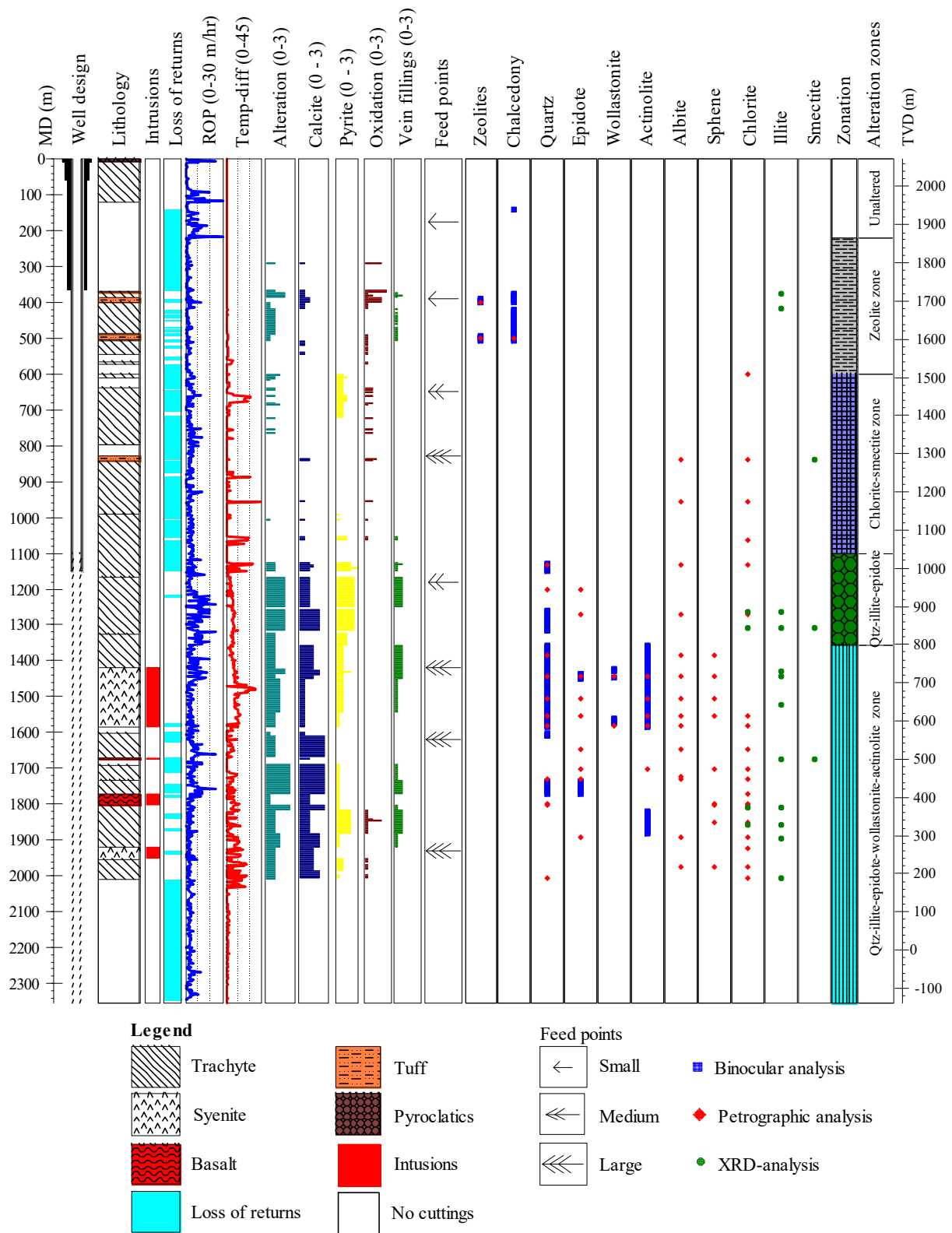


FIGURE 8: Lithology, distribution of hydrothermal alteration minerals, mineral zonation and location of aquifers in well MW-19A


Crystallinity of the host rock is of importance because glass is more easily altered than crystalline rock. The chemical composition of the host rock determines the availability of components to form alteration minerals as well as possible fugitive components from the presumed magmatic heat source. Temperature is the most significant factor in hydrothermal alteration because most of the chemical reactions require elevated temperatures and also minerals are thermodynamically stable at high temperatures (Lagat et al., 2005) Pressures at the depths penetrated by well MW-19A drill hole, like any other geothermal fields elsewhere in the world are not sufficient to greatly affect hydrothermal alteration minerals transformation (Browne and Ellis, 1970; Lagat et al., 2005).

The main hydrothermal minerals in Menengai geothermal field are calcite, zeolites (e.g. scolecite), chlorite, chalcedony, epidote, actinolite, wollastonite, secondary iron oxides (e.g. magnetite), sulfides (e.g. pyrite and chalcopyrite) and quartz. Mineral associations in vesicles are common and consist of two or more of the alteration minerals with the paragenetic sequence varying with depth and from one well to another.

### 5.1 Alteration of primary minerals

Most of the primary rock forming minerals are unstable in a geothermal environment and are, therefore susceptible to replacement by new minerals that are either stable or at least metastable under the new conditions. Although hydrothermal alteration has changed the primary minerals in different ways and magnitude, often the original textures of the minerals are still recognizable. The primary minerals found in MW-19A include volcanic glass, quartz, olivine, pyroxene, amphibole, feldspars, and opaque minerals (FeTi-oxides). Glass shows little alteration at shallow depths but is completely altered down the well, whereas quartz apparently shows little or no alteration at all. Feldspars, pyroxenes, and iron oxides show a greater resistance to alteration compared to glass and olivine. Sanidine and plagioclase are the main feldspars in this well. In thin sections, the sanidines appear fine grained and elongated, exhibiting the trachytic texture. It also occurs both in the groundmass and as phenocrysts exhibiting porphyritic textures. The sanidine phenocrysts were readily identified by low relief and simple twinning. At shallow depths, the feldspars are relatively unaltered but become progressively altered with depth into albite and occasionally to clays, calcite, and epidote. Albite, epidote and sphene are observed to partly replace plagioclase below 800 m. Olivine is rare in this wells and occurs as greenish anhedral crystals with polygonal outlines. It is distinguished by its poor/lack of cleavage and high birefringence under the petrographic microscope. Olivine shows alteration to oxides and clays. In most cases it is completely altered and its presence is revealed by the outline of the alteration product. Fe-Ti Oxides are the most abundant opaques in this well and are relatively resistant to alteration. These oxides occur as magnetite and mostly alter to sphene. Table 1 below summarizes the order of replacement of the primary minerals and their alteration products in the well.

TABLE 1: Order of replacement of primary minerals and their alteration products (modified from (Browne, 1984))

Primary minerals		Replacement products
Volcanic glass	 Increasing order of replacement	Zeolites, quartz, calcite, clays
Pyroxenes, amphiboles, olivines		Chlorite, illite, quartz, pyrite, calcite
Sanidine, orthoclase, microcline		Calcite, adularia, chlorite, illite,
Ca-plagioclase		Calcite, albite, adularia, chlorite, illite, sphene, quartz, epidote
Iron oxides		Pyrite, sphene, secondary oxides



## 5.2 Description and distribution of hydrothermal alteration minerals in well MW-19A

The distribution of hydrothermal minerals in well MW-19A is shown in Figure 8. At shallow depths, low temperature minerals are seen to dominate with mainly zeolites, chalcedony, amorphous silica, calcite, oxides, clays (smectite and chlorite) and sulphides being the minerals present. In the deeper parts of the well, hydrothermal alteration is seen to range from moderate to high. Quartz, epidote, pyrite, calcite, wallastonite, albite, sphene, illite, chlorite and actinolite are the alteration minerals here.

Generally, the hydrothermal alteration pattern shows prograde alteration with increase in temperature and depth with the low temperature mineral assemblages disappearing as the high temperature assemblages appear. However, actinolite, which is a high temperature alteration mineral was observed at 1358 m depth where the current measured formation temperature is 226°C. This mineral now exists where the present temperature is much lower than its expected thermal stability range (>290°C) indicating that the temperatures at this section at one time must have been higher than the present temperatures and therefore the mineral is considered relict. Below is a brief description of the hydrothermal alteration minerals encountered in MW-19A.

*Zeolites* were observed at 142, 402 m and between 494-506 m depths in this well. Two types of zeolites were observed, scolecite and mesolite. They occur as densely packed fibrous aggregates often in hemispherical forms radiating from several sources along vesicle walls, especially in tuff layers. Zeolites are generally thermodynamically metastable at 60-110 °C (Kristmannsdóttir, 1979).

*Chalcedony* is noted from 142 m to around 450 m. It is translucent, often milky or greyish cryptocrystalline form of silica which occurs at temperatures below 120°C mostly in vesicles, vein fillings or fractures. It is characterized by smooth, almost perfectly circular morphology. At greater depths where temperatures are high, chalcedony in vesicles is seen transforming or is completely transformed into quartz but the chalcedonic outline is still preserved.

*Calcite* is ubiquitous in this well and occurs from around 300 m, through to the bottom of the well and is most abundant from 1120 m. This is attributed to increased boiling as a result of high formation temperatures. Calcite presence is associated with carbon dioxide activity in the reservoir which clearly indicates active magmatism. The mineral occurs as deposition vesicles, veins and disseminated in the groundmass where it replaces sanidine feldspar. Crystal morphology of calcite is variable and ranges from individual thin-bladed crystals to equant or needle like crystals.

*Quartz* is colourless to white in colour and occurs in euhedral to subhedral crystals. Quartz is identified both as open space (vesicle) fillings and vein filling mineral. The mineral was first seen at 1128 m depth and persists almost to the bottom of the well with varying intensities. It was easily identified in cuttings by its typical euhedral shape, transparency and forming a regular hexagonal pyramid form. Some of the euhedral grains of quartz were noted growing in clusters while others grew individually. At shallow depths, it was seen replacing chalcedony while at deeper depths it deposited in vesicles, veins and fractures. Its presence in a geothermal system indicates temperatures of above 180°C. (Franzson, 1998).

*Epidote* is one of the main hydrothermal index minerals which often shows a systematic textural development with increasing depth. The first occurrence of epidote in this well is indicated by its greenish colouration forming fine-grained aggregates and later fully develops into yellowish-pale green idiomorphic, tabular, radiate to fibrous crystals. Epidote was first seen in the petrographic microscope at 1202 m. It is found filling fractures, vesicles, and replacing primary plagioclase and pyroxene. In most cases epidote forms mineral associations with mainly quartz, chlorite and sometimes calcite and pyrite. The presence of well-crystallized epidote indicates temperatures above 250°C.

*Wollastonite* is an alteration mineral often associated with contact metamorphism and, therefore, its occurrence is probably related to the numerous intrusions in the caldera summit area (Mibei, 2012).

Wollastonite was observed at 1270 m and was seen to diminish below 1574 m in this well. It is colourless and fibrous under the binocular microscope and indicates temperatures of  $\geq 270^{\circ}\text{C}$ .

*Pyrite* is fairly abundant in MW-19A in comparison to other wells drilled in Menengai and was observed to occur between 600 to 720 m and 1100 to the bottom of the well with varying intensities. It occurs as euhedral cubic crystals with brassy yellow luster in reflected light. Very small cubic pyrite crystals were deposited in fractures, vesicles and veins and as disseminations in the groundmass. Appearance of this mineral is taken to indicate enhanced permeability within the reservoir.

*Actinolite* is green to greyish green in colour, forms radiating fibres or acicular crystals and also massive to granular aggregates in the groundmass and has a moderate birefringence. It's produced as a result of high degree of water rock interaction. Where it occurs alteration is strongest especially near microfractures and veins that were interpreted to be the main fluid conduits. In this well actinolite was encountered between 1358 and 1882 m where intense alteration was also noted. The presence of actinolite indicates temperatures between 280 and  $350^{\circ}\text{C}$ .

*Albite* is a secondary mineral which occurs as an alteration mineral from feldspars. Albitization in this study is referred to replacement of primary K-feldspar and plagioclase phenocryst by hydrothermal albite. Albitized K-feldspar has a low refractive index and shows no zoning but typical microcline-like twinning. Albite alteration occurs at around 800 m but extensive albitization is noted at 1400 m in this well. Below 1,900 m, clear euhedral albite crystals were identified.

*Sphene (titanite)* was observed only in petrographic microscope. In thin section, it was easily identified by its distinct yellow-brown colour, very high relief and its common diamond shape often seen replacing opaque minerals.

*Oxides* form readily in the surface or near surface environment, where oxygen from the atmosphere is more readily available and at the baked contact between the cold and the hot rock. The most common ones to form are mainly iron oxides, but many different types can form, depending on the metal cations present. Sulphide minerals often weather easily because they are susceptible to oxidation and replacement by iron oxides. In this well oxidation was noted from the surface to around 1000 m depth and from 1800 to 2000 m although in minute quantities.

*Clay* minerals have proved very useful mineral geothermometers in the study of many geothermal systems around the world. Mixed-layer clays (illite, smectite and chlorite), kaolin group (two-layer clays) smectite group (three-layer, expanding lattice), illite group (three-layer, non-expanding) and the chlorite group (three-layer with interlayer cations). Typically, clay minerals form microscopic to sub-microscopic crystals (in some cases, crystallinity is totally limited); hence, it becomes a bit complicated to study these minerals under a microscope. In order to compliment petrographic and binocular analysis, X-ray diffraction analysis for 18 samples in well MW-19A was carried out (Table 2). In this analysis the samples were prepared and subjected to three XRD treatments; air-dried, glycolated and then heated. Three types of clay were identified; these are: smectite, chlorite and illite.

*Smectite* is a low-temperature clay and its occurrence is an indication of temperatures lower than  $200^{\circ}\text{C}$ . Smectite is not common in MW-19A. It was positively identified in the XRD analysis at 838-840 m, 1308-1310 m and 1672-1674 m depth (Table 2). It showed peaks commonly occurring between 12.8 and 15 Å when untreated, 13 to 17 Å when treated with glycol and collapsing to 10.3 Å when heated (Figure 1 in Appendix I). The appearance of smectite at 1308-1310 m can therefore be attributed to the temperature reversal observed (see chapter 5.7 in Figure 13b) between 1100 and 1400 m depth in this well while its appearance at greater depths is against the norm where it is found existing where the present formation temperature is much higher than its thermal stability range of  $50\text{-}200^{\circ}\text{C}$ . This may indicate several regimes of geothermal activity or evidence of reduced permeability in this section of the well where it occurs.

TABLE 2: Results of clay minerals identified from XRD analysis

Sample ID	Depth (m)	Untreated (Å)	Glycolated (Å)	Heated (Å)	Type of clay
1	374-376	10.21	10.21	10.21	Illite?
2	416-418	10.21	10.21	10.21	Illite?
3	500-502				No clay
4	540-542				No clay
5	838-840	15.53	17.32	10.02	Smectite
6	992-994				No clay
7	1128-1130				No clay
8	1262-1264	12.70	12.70	7.57	Smectite?
	1262-1264	10.30	10.30	10.30	Illite?
9	1308-1310	12.70	12.70	10.30	Smectite
	1308-1310	10.30	10.30		Illite
	1308-1310	12.70	12.70		Chlorite
10	1426-1428	10.40	10.40	10.26	Illite
11	1440-1442	10.40	10.40	10.26	Illite
12	1522-1524	10.40	10.40	10.26	Illite
13	1602-1604				No clay
14	1672-1674	15.26	17.48	10.26	Smectite
	1672-1674	10.26	10.26	10.26	Illite
15	1808-1810	14.67	7.20		Unstable chlorite
	1808-1810	10.26	10.26	10.26	Illite
16	1856-1858	12.24	12.24	10.19	Smectite?
	1856-1858	10.32	10.32	10.19	Illite
17	1894-1896	10.40	10.40	10.20	Illite
18	2004-2006	10.37	10.37	10.19	Illite

*Chlorite* occurs below 438 m to the bottom of the well. The mineral shows a wide distribution and a big variability in colours, form and textures. It varies in colour from light-to-dark green, has low birefringence and occasionally shows anomalously blue, brown or purple interference colours and presents two different forms. In the upper section of the well, chlorite appears in small intergranular patches whereas at the deepest levels, chlorite is idiomorphic, forming radial aggregates in vein-lets and vugs in association with quartz, calcite, epidote and pyrite. Within veins, chlorite occurs as micro-spherules enclosed within epidote, but it may also replace primary pyroxene, and the matrix. In the study well, chlorite was first identified in the petrographic microscope at 580 m depth and was seen to occur intermittently to the bottom of the well. It exhibits characteristic unchanged peaks of 14.50 and 7.28 Å when untreated and glycolated, and completely collapses after being heated to 550°C. Occurrence of chlorite indicates formation temperatures of over 220°C (Reyes, 2000).

*Illite* is the most common clay mineral group in well MW-19A. In the study well, illite first occurred at 400 m, becomes rare and reappears again from 1444 m to the bottom of the well. It displayed peaks between 10.19-10.40 Å in untreated, glycolated and heated samples (Figures 2, 3 and 4 in Appendix I). Occurrence of illite indicates temperatures greater than 200°C.

### 5.3 Mineral paragenesis

The paragenetic sequences in hydrothermal systems are identified from cross-cutting relationship in veins and mineral fillings in vugs and vesicles. This gives a clear picture on the way the geothermal system has evolved over time as well as predicting its future. The mineral deposition sequence in well MW-19A was rarely observed. However, a few sequences were noted. At shallow depths, zeolites were seen to deposit in vesicles, which later disappeared at around 550 m. Chalcedony on the other hand

which is a low temperature mineral was seen to form in vesicles and later transforming into quartz with depth. At greater depths of 1308 m, well developed quartz crystals were seen overlying calcite in vesicles, but at some instances quartz was observed to form first and calcite deposited later. At around 1748 m, actinolite was seen to form on top of epidote an indication that the system is evolving to higher temperature conditions. This is also evidenced by the measured formation temperatures of 319°C at the same depth.

#### 5.4 Hydrothermal mineral zonation

Hydrothermal conditions found in the reservoir could easily be inferred from a closer look at the hydrothermal mineral assemblages. Occurrence of alteration minerals, whose formation temperatures are known, are useful geothermometers to predict formation temperatures, although some minerals may represent past conditions. In this well the hydrothermal minerals used to determine the zonations are zeolites, smectite, chlorite, quartz, illite, epidote, wollastonite and actinolite. Each zone is characterized by a definite assemblage of hydrothermal minerals and is defined by the first appearance of its index mineral. Based on this study five hydrothermal alteration zones were identified (Figure 8), although there could be a possibility of one or two more sub-zones. Below is a brief description of each of the zones.

*Unaltered zone* which consists mainly of pyroclastics and trachytes showing a high level of oxidation. The rocks in this zone show little or no alteration at all.

*Zeolite zone*: This zone extends from around 220 m to about 502 m. Presence of circulation losses in this section of the well makes it difficult to determine the exact boundaries of the zone. This zone is marked by the presence of chalcedony, calcite, smectite and zeolites and the temperature range is less than 200°C.

*Chlorite-smectite zone*: This zone is made up of an assemblage of clay minerals. It ranges from around 502 m to 1100 m when quartz starts to appear, and characterises a temperature interval of about 180-230°C. Clays are found to occur in a wide temperature range, however, chlorite and illite show a wide temperature range mainly in intermediate to acidic rocks which seems to be the case in this well.

*Quartz-illite-epidote zone*: This zone is marked by the appearance of quartz, illite, smectite, albite, chlorite, calcite, epidote and wollastonite and ranges from 1100 to 1358 m. This zone indicates an alteration temperature of more than 230°C.

*Quartz-illite-epidote-wollastonite-actinolite zone*: It is defined by the appearance of quartz, illite, epidote, wollastonite and actinolite from 1358 m, and persists to the bottom of the well. The appearance of actinolite at this zone reveals formation temperatures of above 280°C (Reyes, 2000).

#### 5.5 Fluid inclusion geothermometry

Fluid inclusion geothermometry is a powerful tool for outlining changes in temperature regimes in a geothermal system (Roedder, 1972). Fluid inclusions are tiny bubbles of liquid and vapour that are formed when fluids are trapped in crystals and subsequently cooled due to differential thermal contraction of fluid and host mineral. Primary inclusions are formed during primary crystal growth, often concentrated along the first order of growth discontinuity or occur as isolated inclusions distributed within the crystal. Secondary inclusions are formed after primary growth, often along healed microstructures (Roedder, 1984). The inclusions in any given sample are seldom of only one generation. In some minerals from hydrothermal deposits, the primary inclusions are sparse and randomly distributed and relatively large, but the secondary inclusions in the same sample are small, very numerous and in planar arrays (Roedder, 1984).

In the present study fluid inclusion micro-thermometric measurements were done on inclusions trapped in a quartz crystal from 1406 to 1408 m depth and calcite crystal from 1748-1758 m depth range in MW-19A, to determine the temperature at which the inclusions were formed. They were heated using a Linkam THSMG 94 freezing and heating stage and the temperatures at which the inclusions reached homogenisation temperature and the bubbles disappeared were noted. The temperature measurements were done in three phases; the first heating phase was done at a rate of 20°C/minute up to 100°C, while the second phase of heating was done at a rate of 10°C/minute up to 200°C and the last heating phase was done at a rate of 5°C /minute until the bubbles disappeared, care being taken to avoid blowing up the inclusions.

In this well a total of 30 inclusions were analysed, 14 and 16 inclusions from quartz and calcite, respectively. The homogenization temperatures obtained from the quartz crystal ranged from 293 to 305°C (Figure 9) with an average value of 298°C while those from calcite ranged from 265 to 310.7°C (Figure 10). The results obtained from calcite varied widely showing two populations. The first population ranged from 265 to 277°C with an average value of 272°C while the second population ranged from 287 to 310.7°C with an average value of 297.7°C. The low temperature values from the first population are therefore assumed to be from secondary inclusions, whilst the higher values from the second population are assumed to be from primary inclusions. The results from this analysis are presented on histograms in Figures 9 and 10.

The  $T_h$  values from inclusions hosted in the quartz crystal gave an average value of 298°C whereas, the measured formation temperature at the same depth is 226°C. The lowest  $T_h$  value of 293°C is 67°C higher than the measured formation temperature and the highest  $T_h$  value (305°C) is 75°C above the measured formation temperature. The average value for inclusions in the quartz crystal is 298°C and is 72°C above the measured formation temperature.

In the calcite crystal, the lowest  $T_h$  value of 266°C from the first population is 53°C lower than the measured formation temperature (319°C) and the highest  $T_h$  value (277°C) from the same population is 42°C lower than the measured formation temperatures. The average value (272°C) of the first population from the calcite crystal is 47°C below the measured formation temperature. In addition, the lowest  $T_h$  values in the second population from the calcite crystal is 32°C lower than the measured formation temperature and the highest  $T_h$  value (310.7°C) is 8.3°C below the measured formation temperature (319°C). The average  $T_h$  value for the inclusions from the second population is 21.3°C below the measured formation temperature. These measurements indicate that the inclusions in the quartz

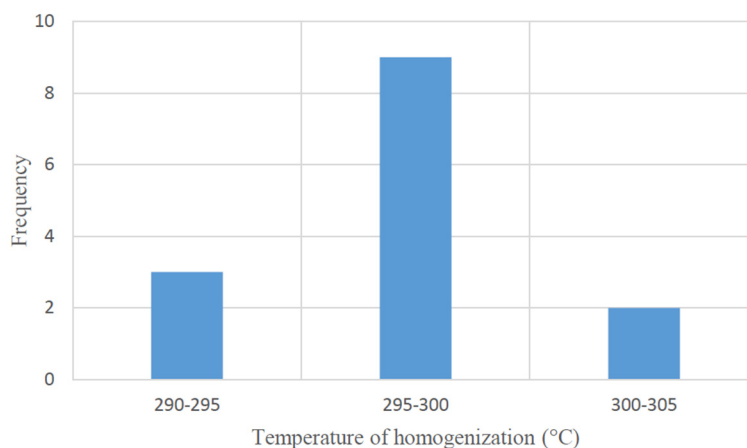


FIGURE 9: Fluid inclusion measurements from quartz crystal (1406-1408 m depth)

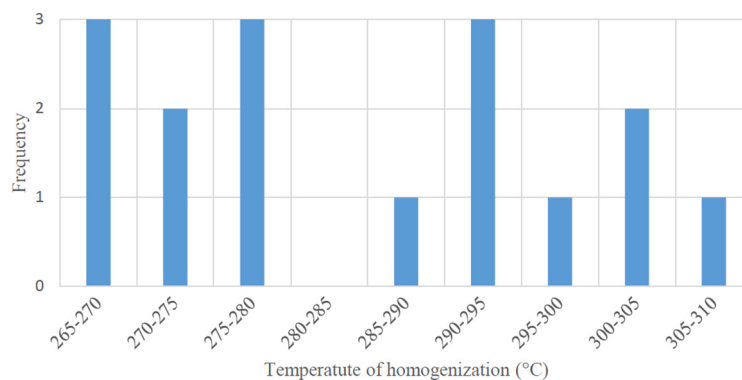


FIGURE 10: Fluid inclusion measurements from calcite crystal (1748-1758 m depth)

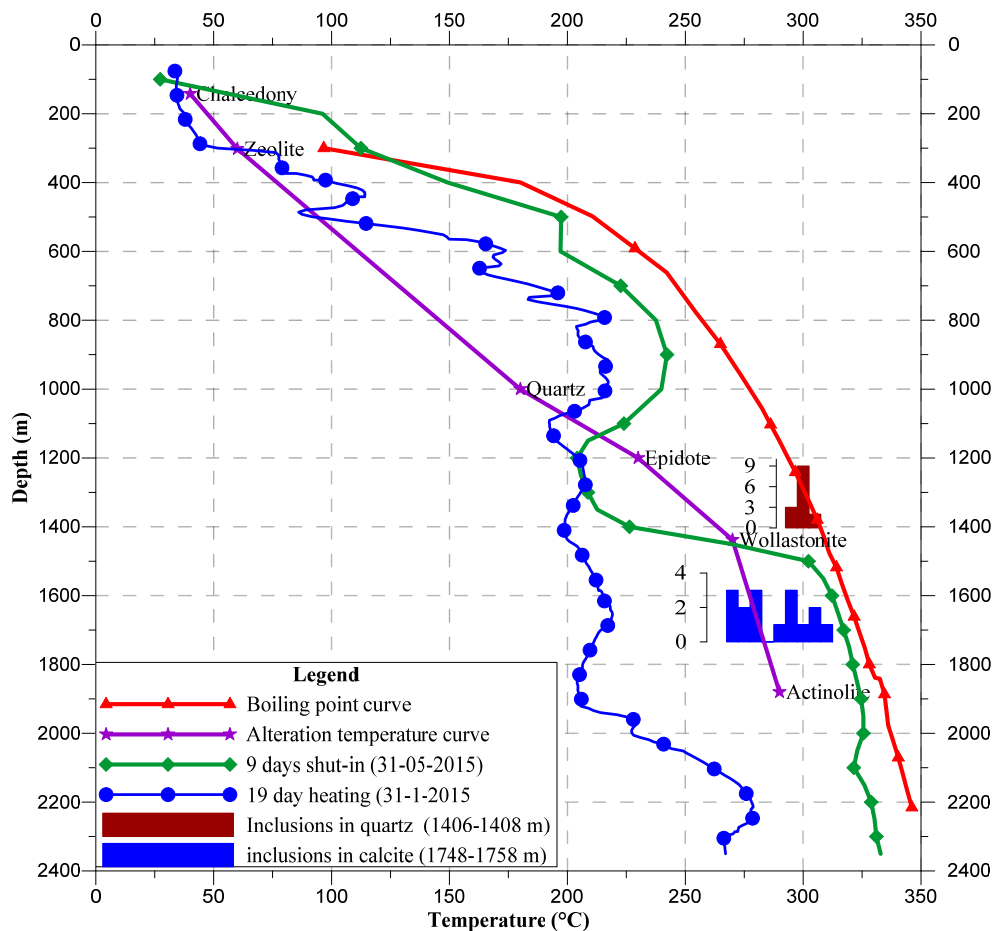


FIGURE 11: Boiling point curve and correlation between measured, interpreted hydrothermal alteration minerals and fluid inclusion temperatures with depth of well MW-19A

precipitated from a hotter fluid implying a much hotter conditions in the past. Moreover, the inclusions in the first population from calcite indicate that the fluids in these inclusions were trapped from a much cooler fluid at a later stage whereas the fluid from the second population from the calcite crystal indicate that the fluid in this inclusions were trapped in a more or less the same temperatures as the current formation temperatures hence the system at this point is either heating up or at equilibrium. Generally, the fluid inclusion analysis indicate an increase in temperature with depth.

Results from fluid inclusions from well MW-19A were integrated together with the measured, alteration and boiling point temperature curves (Figure 11), so as to understand how the geothermal system has evolved with time. The correlation between the alteration temperature, measured formation temperature and fluid inclusions in this well indicate cooling between 1100 and 1400 m with hydrothermal minerals occurring below their stability range. For example, actinolite was seen to form before wollastonite (Figure 8) where the formation is below its temperature stability range indicating it is relict. Below 1400 m and to the bottom of the well, the measured formation temperature is greater than both the alteration and fluid inclusions temperature and almost close to the boiling point curve. Therefore, it appears that the system is heating up, or possibly approaching equilibrium, with the mineral assemblages in this zone occurring within their temperature stability ranges.

## 5.6 Aquifers / permeable zones

For a hydrothermal system to exist, permeable formations or structures should exist to allow hot water to percolate through. These permeable zones form the aquifers (Lagat, 2004). Typically, aquifers are

located at the intersection of faults, fractures, intrusions and lithological contacts. In a geothermal system, aquifers can either be cold or hot. The cold aquifers, which are usually encountered in the upper parts of the wells, are cased off and carefully cemented to prevent them from cooling the hot aquifers in the deeper part of the wells. Permeable zones in MW-19A were interpreted based on various parameters, which include; the rate of penetration (ROP), loss of circulation, differential temperature in the circulation fluid during drilling, lithological contacts and hydrothermal alteration mineralogy patterns as well as temperature logs.

Indicators of high permeability in MW-19A, apart from high alteration intensity and sheared rocks (fractures), include the presence of abundant pyrite and calcite. These minerals are commonly found in or adjacent to aquifers penetrated by the well and occur as alteration of the rocks as well as in veins, often as coarse grains. Low permeability on the other hand, apart from absence of the above minerals, is indicated by relatively fresh rock indicating low water rock interaction and presence of blocked veins. However, based on the above mentioned parameters, MW-19A is a very permeable well and eight possible permeable locations were identified at 150-200, 388-400, 620-680, 836-842, 960, 1460-1500, and 1920-1980 m depths (Figures 12). Table 3 below gives a brief summary of the possible permeable zones identified in the well.

Minor loss or gain in circulation could not be established because the volume of circulation fluid coming out of the well-bore was not being measured during drilling, therefore small aquifers could not be identified. Circulation losses recorded at shallow depths above the groundwater table were attributed to blocky trachytic lavas but most of these zones, including the unwanted cold aquifers, were cased off. Generally, the identified permeable locations can be grouped into four major aquifers (Figure 12). Production casing in this well was positioned at 1150.1 m RKB depth. Therefore, the upper two aquifers were cased off to avoid quenching of the deeper hot aquifers. However, the second aquifer was partly cased as evidenced by the temperature reversal from the temperature logs (Figure 13b).

TABLE 3: Interpreted permeable zones and aquifers/feed zones based on geological observations and fluid circulation temperature measurements

Depth	Evidence from geological observations, drilling observations and temperature monitoring profiles (logs)
150-200	Major circulation loss, high rate of penetration, increase in measured temperature
388-400	Primary permeability in tuff, circulation loss, increase in alteration intensity and oxidation, increase in measured temperature
620-680	Circulation loss, relatively high penetration rates, increase in alteration intensity and oxidation, increase in measured temperature, abundance of pyrite
800-860	Primary permeability in tuff, major circulation loss, increase in measured temperature
1110-1300	Major circulation loss, abundance of calcite and pyrite, decrease (reversal) in measured temperature
1460-1500	Lithological contact between trachyte and syenite, increase in alteration intensity, increase in measured temperature, abundance of calcite and pyrite, fractured formation
1770-1800	Lithological contact between trachyte and basalt, increase in alteration intensity, increase in measured temperature, abundance of calcite and pyrite, fractured formation
1920-1980	Lithological contact between trachyte and syenite, increase in alteration intensity, increase in measured temperature, abundance of calcite and pyrite,

### 5.7 Correlation of MW-19A and other wells (MW-19, MW-22 and MW-11)

A lithologic cross-section across wells MW-19A, MW-22 and MW-11 is presented in Figure 12a below. The section reveals to some extent the subsurface geology and the structural system of the north western part of the caldera and partly part of the area around the caldera summit. The lithology of MW-19A shows some similarity to that of some previously studied wells in Menengai. The top most section is

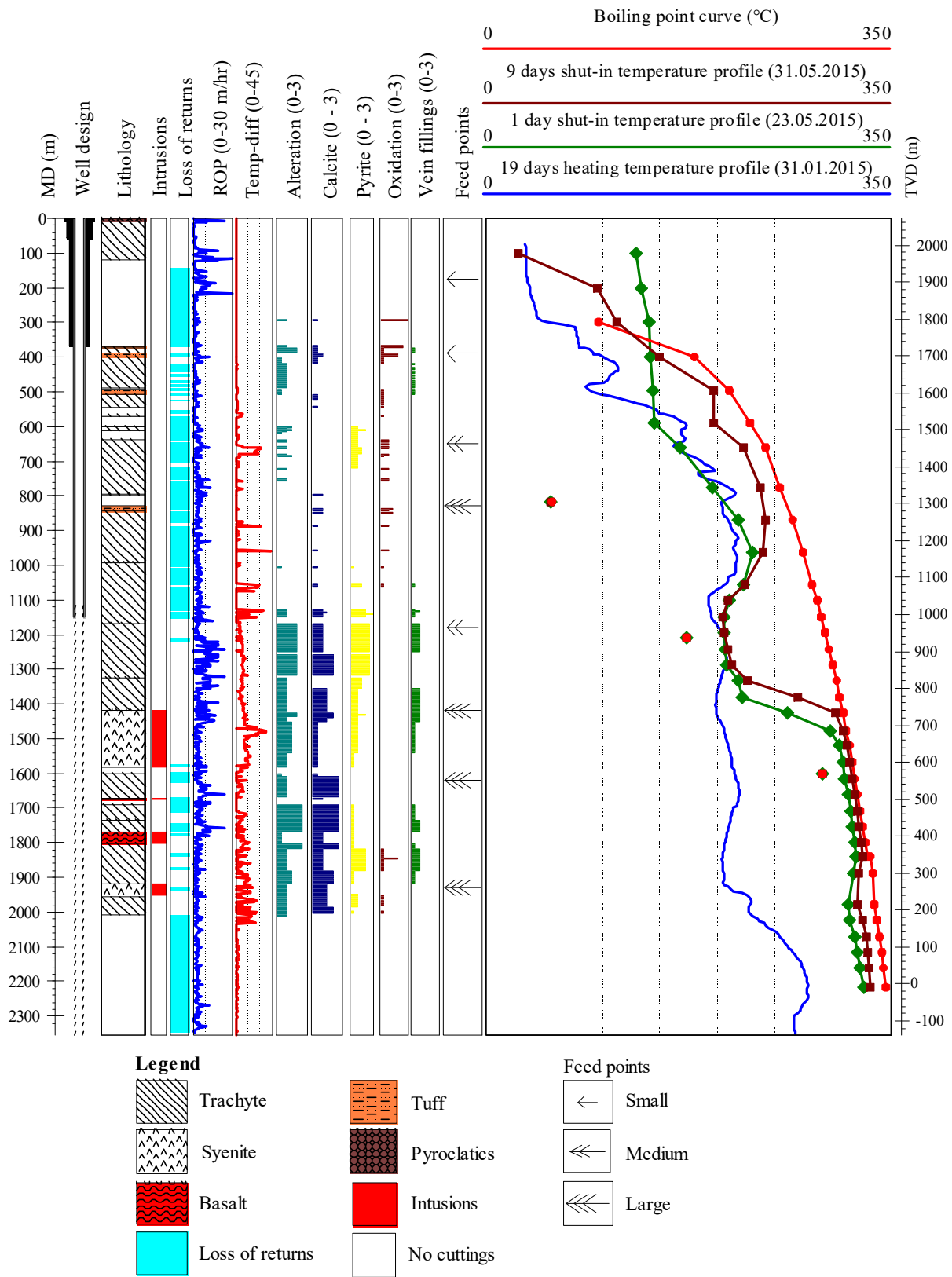


FIGURE 12: Lithology, selected alteration minerals and temperature logs in correlation with aquifers in well MW-19A



mostly composed of mainly unconsolidated pyroclastics. The pyroclastic unit is seen to thin towards the caldera summit area and this can be associated with erosion since the area is topographically high but thickens towards well MW-11.

Four major tuff marker horizons were identified in MW-19A (Figure 13a), which possibly demarcate the boundaries between post-, syn- and pre-caldera volcanics. These markers are defined by tuffs encountered at 368-372 m, 388-400 m, 492-504 m and 836-842 m in MW-19A.

These markers were also encountered in well MW-11, but only one marker horizon was encountered in well MW-22. This is attributed to the total circulation loss experienced in the well, hence no samples were recovered making a correlation difficult. The first two tuff markers are believed to have been emplaced during the syn-caldera activity whilst the other two were emplaced during the pre-caldera phase in tandem with what Leat (1984) reported. Basalt on the other hand was intersected in both wells MW-19A and MW-11, but it was not intersected in MW-22. Kipchumba (2013) presumed that the basaltic intrusions were linked to the Pliocene and Pleistocene subordinate basalts overlying the Miocene phonolites, resting on the Precambrian basement, described by Leat (1984). Syenite was only intersected in well MW-19A and MW-22. Syenite in MW-19A was encountered at a shallower depth compared to MW-22. This could possibly be interpreted to have been caused by complex intrusive activity that resulted to the doming underneath the central part of the caldera at 2 km depth (GAB, 2013, Mbia, 2014). From lithologic correlation we can infer the possibility of the existence of normal faults between these three wells.

From the temperature logs (Figure 13b), cold inflow is observed in all the three wells. In well MW-19A it is noted between 1100 and 1380 m, while in MW-22 and MW-11 the cold inflow is seen to occur at

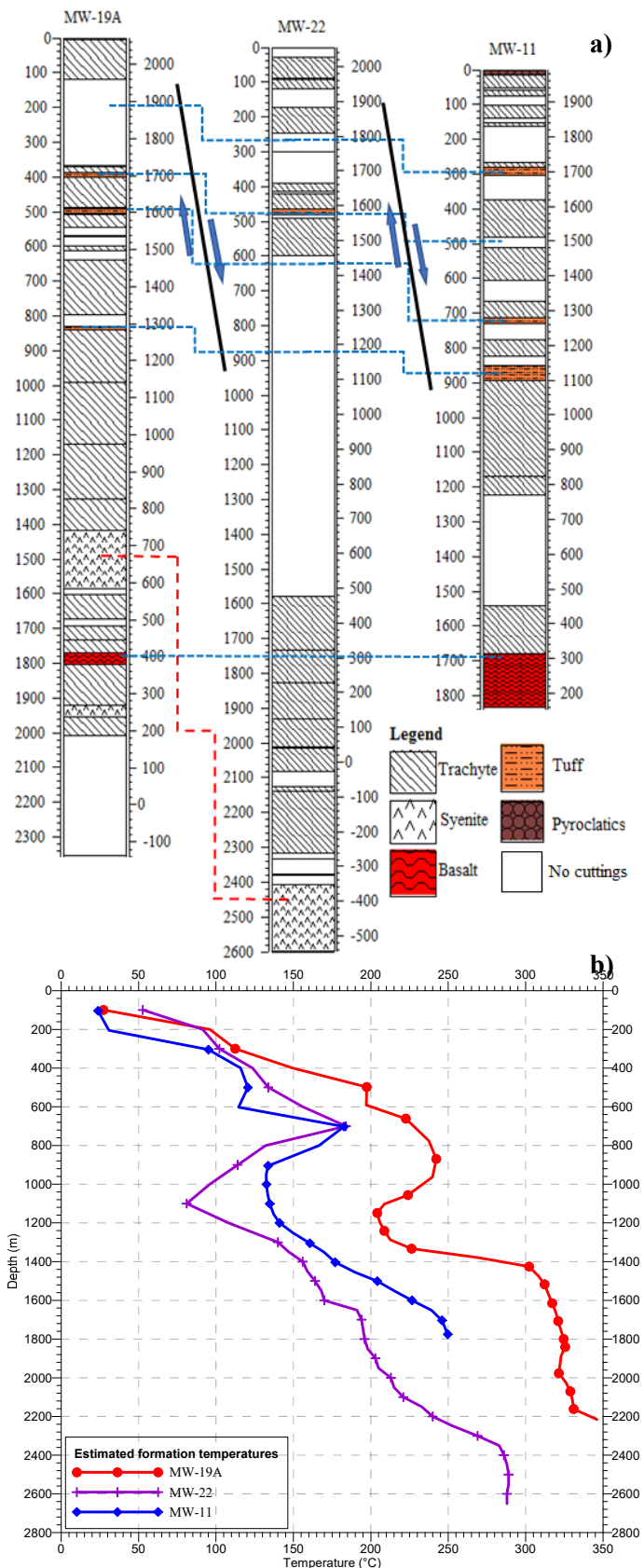


FIGURE 13: Comparison plots of lithologic cross-section (a) and estimated formation temperatures of wells MW-19A, MW-22 and MW-11 (b)

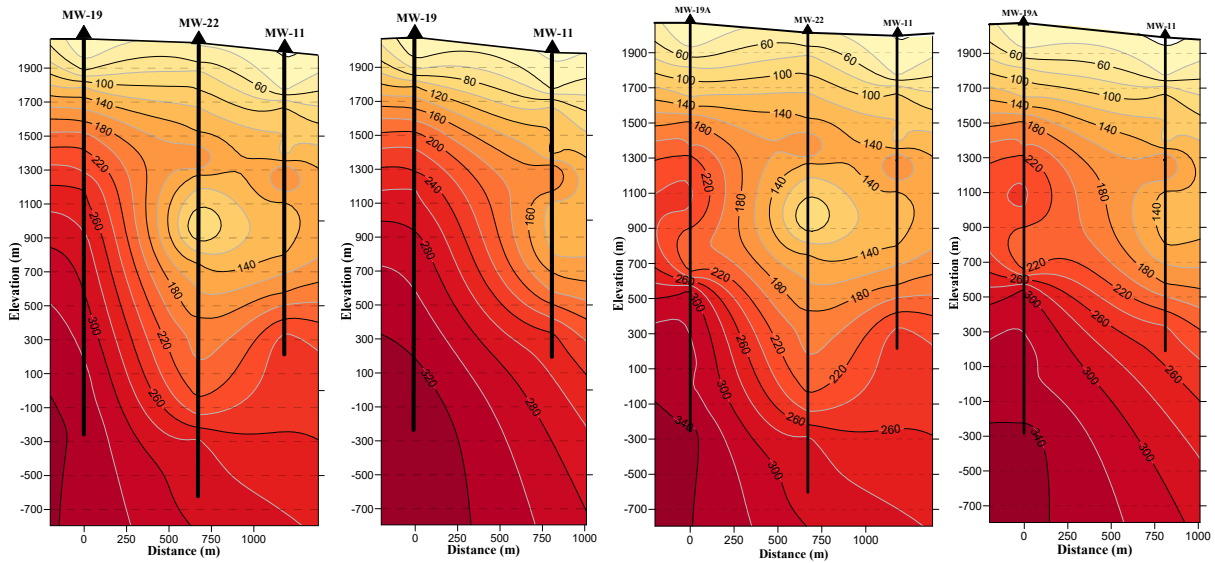


FIGURE 14: Correlation of estimated formation temperatures between wells MW-19, MW-19A, MW-22 and MW-11

almost the same depth but at a shallower depth as compared to MW-19A. This could be attributed to the occurrence of a young underlying structure which could be channelling cold water into the wells.

In an attempt to understand better the sub-surface structural controls in this part of the caldera, a correlation was completed (Figure 14) between the measured formation temperatures in the three wells. From Figures 14a and 14c it is clear that a structure exists between well MW-22 and MW-11 which correlates very well with lithologic interpretation in addition to the persistent loss of circulation experienced in this section of the wells. The cross-section between the vertical well MW-19 and MW-11 (Figure 14a) also confirms the existence of same structure since the cold inflow is seen occurring near well MW-11, while in Figure 14d the effects of the cold inflow in the study well MW-19A drilled towards MW-11 is also seen to occur confirming that a structure is controlling this cold incursion. Therefore, the cold inflow in this wells can be attributed to the extrapolated E-W trending structure (Figure 15) mapped by Strecker et.al. (2013) on the surface near well MW-8 and seems to extend

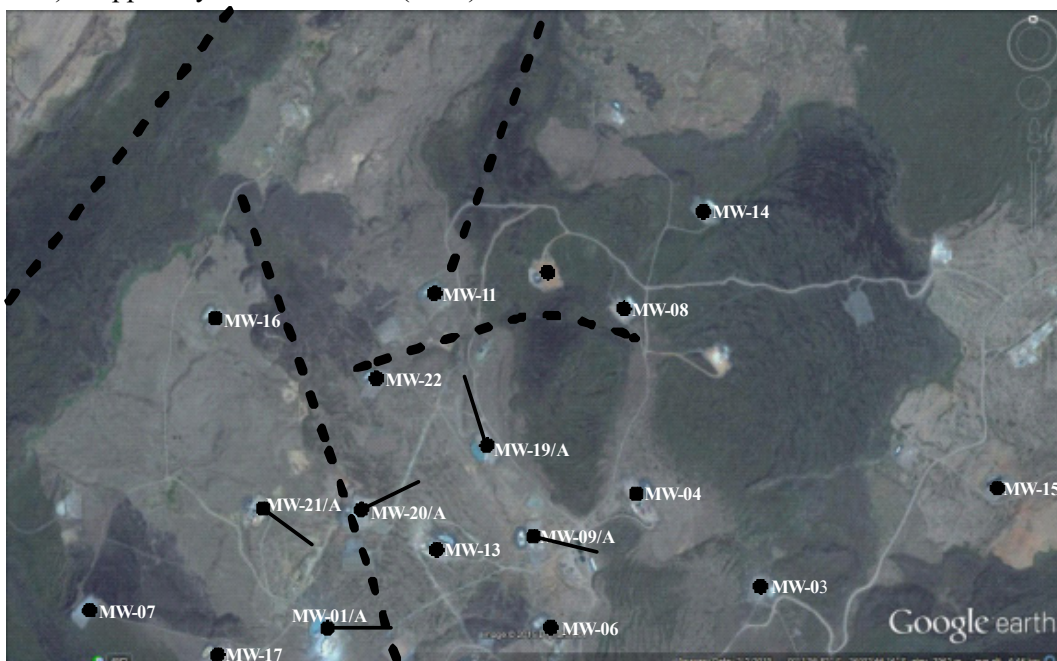


FIGURE 15: Inferred faults north of MW-19/A

towards well MW-11. In the present study, this structure has been extrapolated to form an arc like fissure towards well MW-22 following the topography assumed by the lavas which emanated from the same structure. Another structure that can be associated with the cold inflow is the N-S trending structure north of well MW-11. Since the two structures seem to converge somewhere between well MW-22 and MW-11 it can be interpreted that the structures here act as a trap of cold surface water which in turn finds its way to the nearby wells. This is supported by the inferred faults in the lithologic cross-section although more data is deemed necessary to validate the exact positions and the occurrence of these faults. In this light, it is recommended that deeper production casing of the wells around this area need to be considered in future to prevent the cold inflow.

## 6. DISCUSSION

The lithology of MW-19A was interpreted by analysing the drill cuttings from the well using binocular and petrographic microscopes. From these analyses, five main rock types, pyroclastics, tuffs, trachytes, basalts and syenite were encountered in the well. Pyroclastic rocks form the uppermost 6 m while the underlying formation is formed by trachyte, which is the dominant rock alternating with pyroclastics, tuff, basalt and syenite. The trachyte showed varied textures in the well column, which could indicate different episodes of lava eruptions during the pre-caldera volcanic phase, an observation made by Mibei (2012) and Kipchumba (2013). Four major tuff marker horizons were identified in MW-19A, which possibly demarcate the post, syn- and the pre-caldera volcanics.

Hydrothermal alteration minerals are observed in veins, vugs and vesicles and as a replacement of primary minerals. Their distribution pattern shows prograde alteration with increasing temperature and depth. The hydrothermal alteration minerals observed in this well include, zeolites, chalcedony, calcite, chlorite, pyrite, quartz, epidote, albite, sphene, wollastonite and actinolite. The study of the hydrothermal distribution pattern shows five distinct alteration zones with the first appearance of index alteration minerals coinciding with the upper boundary of each zone. These are: the unaltered zone (0-220 m) that has no alteration related to geothermal activity, suggesting temperatures of  $<40^{\circ}\text{C}$ . The second zone (zeolite zone) that extends from 220 to 502 m is the lowest grade mineral alteration zone indicating alteration temperatures of  $<200^{\circ}\text{C}$ . It is characterised by high oxidation, chalcedony, calcite and zeolites. The third zone (chlorite-smectite zone), which is marked by the first appearance of chlorite, occurs between 502 and 1100 m. This zone is highly fractured as evidenced by loss of circulation during drilling and is characterised by high oxidation and the presence of pyrite and calcite, suggesting the zone is highly permeable. Quartz-illite-epidote zone is the fourth zone, extending from 1100 to 1358 m. The top depth is marked by the first appearance of quartz, and it is characterised by high intensity of alteration, veining, abundance of pyrite and calcite, indicating that the zone is also highly permeable. The appearance of epidote in this zone indicates that the alteration temperature at 1202 m and below could be above  $230^{\circ}\text{C}$ . Other minerals present in this zone include albite, chlorite, illite, pyrite and calcite. The fifth zone extends from 1358 m to bottom of the well. It is marked by first appearance of actinolite at 1358 m, indicating temperatures above  $290^{\circ}\text{C}$  below this depth. It is characterised by the mineral assemblage of actinolite, wollastonite, epidote and quartz. Other minerals in this zone include pyrite, calcite, chlorite, illite, albite, sphene and oxides.

Observations made from the distribution of hydrothermal alteration minerals, alteration intensity, oxidation trends, veining and temperature logs in well MW-19A indicate that the well is highly permeable and that this permeability acts as fluid flow channels in the rock formations. The presence of abundant calcite and pyrite in the well indicates high past or present permeability. Eight permeable locations were identified in MW-19A and were further grouped into four major aquifers. Circulation losses also play an important part in positioning of the aquifers. The aquifers in well MW-19A are mainly associated with high intensity of alteration, lithological boundaries, highly fractured rocks and associated underlying structures.

Correlation of fluid inclusion analyses, alteration and formation temperatures indicate two geothermal episodes; one of a high temperature geothermal system below 600 m depth to the bottom of the well and a recent second phase of cooling between 1100 and 1400 m. A reversal in formation temperatures is observed between this depth range indicating an incursion of cold fluids. A similar observation is observed in both well MW-22 and MW-11. However, observations made from hydrothermal alteration mineralogy and mineral deposition sequence do not show temperature reversal hence signs of cooling are not evident. This probably implies that the cooling phase observed in this part of the well is a relatively recent event.

## 7. CONCLUSIONS

The following conclusions can be drawn from the present study on well MW-19A:

- I. The lithology of well MW-19A is composed of five different rock units; trachyte, tuff, pyroclastics, basalt and syenite, trachyte being the most dominant.
- II. Hydrothermal alteration mineral assemblages and their distribution in the well are mainly controlled by temperature, rock type, fluid composition and permeability. The shallow section of the well is characterized by low-temperature hydrothermal alteration minerals which evolve to form high-temperature ones at greater depths.
- III. Five alteration zones were identified, based on hydrothermal mineral assemblages. These include; unaltered zone, zeolite zone, chlorite-smectite zone, quartz-illite-epidote zone and quartz-illite-epidote-wollastonite- actinolite zone.
- IV. Well MW-19A is very permeable. Eight permeability zones were identified; these were further grouped to form four main aquifers. Aquifers in this well show close association with circulation losses, temperature logs, fractured formations, lithological contacts between formations and intrusions at depth. High past and present permeability in this well is indicated by the high abundance of pyrite and calcite, high alteration intensity, oxidation, fracturing and occurrence of veins.
- V. Stratigraphic correlation of wells MW-19A, MW-22 and MW-11 indicates the possibility of existence of a normal faulting between MW-19A and MW-22, and MW-22 and MW-11.
- VI. Comparison between fluid inclusion, alteration, and formation temperature indicate evidence of two geothermal phases in the proximity of the well; the first phase of elevated temperatures succeeded by a cooling phase between 1100 and 1400 m CT. Production casing in this well was positioned at 1150.1 m RKB depth. Therefore, deeper production casing of the wells around this area is recommended to be considered in future to prevent the cold inflow.
- VII. Observations made from hydrothermal alteration mineralogy and mineral deposition sequence do not show temperature reversal hence signs of cooling is not evident. This could may imply the cooling of area around the well is a recent event.

## ACKNOWLEDGEMENTS

I would like to express my gratitude to the Government of Iceland and the United Nations University Geothermal Training Programme (UNU-GTP) for giving me the opportunity to take part in the six months course. I would also like to thank Geothermal Development Company (GDC) for granting me the opportunity and time to undertake this noble training.

I am so grateful to the entire UNU-GTP staff: Mr. Lúdvík S. Georgsson, Director, Mr. Ingimar G. Haraldsson, Deputy director, Ms. Málfríður Ómarsdóttir, Ms. Thórhildur Ísberg and Mr. Markús A. G. Wilde for their guidance, time and help in various capacities that made the whole training successful. I am greatly indebted to my supervisor Dr. Björn S. Hardarson for his patience and time to guide me

throughout the project period. My deep and sincere gratitude to the entire Iceland GeoSurvey (ÍSOR) staff, in particular Dr. Hjalti Franzson, Mr. Sigurður S. Jónsson, Ms. Signý and not forgetting Dr. Eniko Bali of the University of Iceland, for taking time off from their busy schedules to share their skills and knowledge with me. Special thanks also go to Ms. Rósa S. Jónsdóttir, for availing literature material at a time when I needed them.

I would finally like to thank the 2015 UNU-GTP fellows most specifically the geothermal geologists (António Luis Peixoto Franco, Patrick Kant Muanza, Davar Ebrahimi, and Hamda Hassan Wais) for the memorable moments, and continuous support with information and ideas whenever needed.

Special thanks to my entire family and friends back home in Kenya for their encouragement and prayers. My deepest appreciation goes to my wife, Juliet, my son, Ethan for their patience, sacrifice, support and for enduring my long absence.

Lastly, I give thanks to God for his sufficient grace, divine favour and blessings upon my life.

## REFERENCES

- Browne, P.R.L., 1984: Subsurface stratigraphy and hydrothermal alteration of the eastern section of the Olkaria geothermal field, Kenya. *Proceedings of the 5<sup>th</sup> New Zealand Geothermal workshop, Auckland, New Zealand*, 33-41.
- Browne, P.R.L., and Ellis, A.J., 1970: The Ohaki-Broadlands hydrothermal area, New Zealand: mineralogy and related geochemistry. *Am. J. Sci.*, 269, 97-131.
- Burke K., and Dewey J., F. 1973: Plume generated triple junctions: Key indicators in applying plate tectonics to old rocks. *J. Geol.*, 81, 406-433.
- Dunkley, P.N., Smith, M., Allen, D.J. and Darling, W.G., 1993: *The geothermal activity and geology of the northern sector of the Kenya Rift Valley*. British Geological Survey Research Report SC/93/1.
- Franzson, H., 1998: Reservoir geology of the Nesjavellir high-temperature field in SW-Iceland. *Proceedings of the 19<sup>th</sup> Annual PNOC-EDC Geothermal Conference, Manila, Philippines*, 13-20.
- GAB, 2013: *Geothermal Advisory Board (GAB) report*. Geothermal Development Company (GDC), internal report, 67 pp.
- GDC, 2010: *Menengai geothermal prospect, an investigation for its geothermal potential*. Geothermal Development Company (GDC), Nakuru, Kenya, Geothermal Resource Assessment Project, internal report, 44 pp.
- GDC, 2015: *Geothermal Development Company (GDC) - A Brief*. Geothermal Development Company (GDC), internal report, 1 pp.
- Geotermica Italiana Srl., 1987: *Geothermal reconnaissance survey in the Menengai-Bogoria area of the Kenya Rift Valley*. UN (DTCD)/Government of Kenya, report.
- Gichira, J.M., 2012: Joint 1D inversion of MT and TEM data from Menengai geothermal field, Kenya. Report 11 in: *Geothermal training in Iceland 2011*. UNU-GTP, Iceland, 137-167.
- Griffith, P.S., 1980: Box fault systems and ramps: A typical association of structures from the eastern shoulder of the Kenya rift. *Geol. Mag.*, 117, 579-586.

Griffith, P.S., and Gibson, I.L., 1980: The geology and the petrology of the Hannington trachyphonolite formation, Kenya Rift Valley. *Lithos*, 13, 43-53.

Jones, W.B., 1985: Discussion on geological evolution of trachytic caldera and volcanology of Menengai volcano, Rift Valley, Kenya. *J. Geol. Soc. London*, 142, 711-712.

Jones, W.B., and Lippard, S.J., 1979: New age determination and geology of Kenya rift – Kavirondo rift junction, west Kenya. *J. Geol. Soc. London*, 136, 63 pp.

Kahiga, E. W., 2014: Borehole geology and hydrothermal alteration mineralogy of well MW-13, Menengai geothermal field, Kenya. Report 16 in: *Geothermal training in Iceland 2014*. UNU-GTP, Iceland, 261-294.

KenGen, 2004: *Menengai volcano: Investigations for its geothermal potential*. Kenya Electricity Generating Company (KenGen), Kenya, Geothermal Resource Assessment Project, unpublished report.

Kipchumba, J. L., 2013: Borehole geology and hydrothermal alteration of wells MW-08 and MW-11, Menengai geothermal field, Kenya. Report 10 in: *Geothermal training in Iceland 2013*. UNU-GTP, Iceland, 143-176.

Kipng'ok, J., 2011: Fluid chemistry, feed zones and boiling in the first geothermal exploration well at Menengai, Kenya. Report 15 in: *Geothermal training in Iceland 2011*. UNU-GTP, Iceland, 281-302.

Kristmannsdóttir, H., 1979: Alteration of basaltic rocks by hydrothermal activity at 100-300°C. In: Mortland, M.M., and Farmer, V.C. (editors), *International Clay Conference 1978*. Elsevier Scientific Publishing Co., Amsterdam, 359-367.

Kuria, Z.N., and Woldai, T., 2003: *Groundwater exploration: A case study of the location of well field north of Nakuru town, Rift Valley Province, Kenya*. Unpublished report, 15 pp.

Lagat, J.K., 2004: *Geology, hydrothermal alteration and fluid inclusion studies of the Olkaria Domes geothermal field, Kenya*. University of Iceland, MSc thesis, UNU-GTP, Iceland, report 1, 79 pp.

Lagat, J.K., Arnórsson, S., Franzson, H., 2005: Geology, hydrothermal alteration and fluid inclusion studies of Olkaria Domes geothermal field, Kenya. *Proceedings of the World Geothermal Congress 2005, Antalya, Turkey*, 14 pp

Leat, P.T., 1983: *The structural and geochemical evolution of Menengai caldera volcano, Kenya Rift Valley*. University of Lancaster, UK, PhD thesis, 482 pp.

Leat, P.T., 1984: Geological evolution of the trachytic caldera volcano Menengai, Kenya Rift Valley. *J. Geol. Soc. London*, 141, 1057-1069.

Lopeyok, T.P., 2013: Borehole geology and hydrothermal mineralization of wells MW-09 and MW-11, Menengai geothermal field, Kenya. Report 15 in: *Geothermal training in Iceland 2013*. UNU-GTP, Iceland, 289-324.

MacDonald, R., and Scaillet, B., 2006: The central Kenya peralkaline province: insights into the evolution of peralkaline salic magmas. *Lithos*, 91, 59-73.

MacDonald, R., Bailey, D. K., and Sutherland, D., 1970: Oversaturated peralkaline glassy trachyte from Kenya. *J. Petrology*, 11, 507-517.

Mbia, P.K., 2014: *Sub-surface geology, petrology and hydrothermal alteration of Menengai geothermal field, Kenya*. University of Iceland, MSc thesis, UNU-GTP, Iceland, report 1, 96 pp.

- McCall, G.J.H., 1957a: The Menengai caldera, Kenya Colony. *20th International Geological Congress, section 1*, 55-69.
- McCall, G.J.H., 1957b: *Geology and groundwater conditions in the Nakuru Area*. Ministry of Water, Hydraulic Branch, Nairobi, technical report 3, 36 pp.
- McCall, G.J.H., 1964: Froth flows in Kenya. *Geol. Rundsch.*, 54, 1148-1195.
- McCall, G.J.H., 1967: *Geology of the Nakuru-Thomson's Falls-Lake Hannington area*. Geological Survey of Kenya, report 78, 122 pp.
- Mibei, G., 2012: Geology and hydrothermal alteration of Menengai geothermal field. Case study: Wells MW-04 and MW-05. Report 21 in: *Geothermal training in Iceland 2013*. UNU-GTP, Iceland, 442-448.
- Omenda, P.A. (editor), 2000: *Ranking of the geothermal prospects in the Kenya Rift Valley*. Contributions from: Lagat, J., Mungania, J., Mariita, N., Onacha, S., Simiyu, S., Opondo, K., Kubo, B.P., Ouma, P., Wetangula, G., and Kollikho, P., KenGen – Kenya Electricity Generating Company, Kenya, internal report, 121 pp.
- Omondi, C., 2011: Borehole geology and hydrothermal mineralisation of wells MW-01 and MW-02, Menengai geothermal field, Central Kenya Rift valley. Report 30 in: *Geothermal training in Iceland 2011*. UNU-GTP, Iceland, 737-773.
- Reyes, A.G., 2000: *Petrology and mineral alteration in hydrothermal systems. From diagenesis to volcanic catastrophes*. UNU-GTP, Iceland, report 18-1998, 77 pp.
- Roedder, E., 1972: Composition of fluid inclusions. In: Fleischer, M. (technical editor), *Data of geochemistry*. Geological survey of America, Washington DC, United States, 199 pp.
- Roedder, E., 1984: *Fluid inclusions*. Mineral. Soc. Am., Rev. Mineral., 12, Washington, DC, 7 pp.
- Schwonke, F., 2009: *High-resolution airborne thermal infrared remote sensing for geothermal site characterization. Geothermal exploration at Menengai-Olbanita prospect, Republic of Kenya*. Bundesanstalt für Geowissenschaften und Rohstoffe (BGR), Germany, 1 pp.
- Simiyu, S.M., and Keller, G.R., 1997: Integrated geophysical analysis of the East African plateau from gravity anomalies and recent seismic studies. *Tectonophysics*, 278, 291–314.
- Strecker, M.R., Blisniuk, P.M., and Eisbacher, G.H., 1990: Rotation of extension direction in the Central Kenyan Rift. *Geology*, 18, 299.
- Strecker, M.R., and Melnick, D., Riedl, S., Njue, L., Mibei, G., Mutonga, M., 2013: *Structural characteristics of Menengai caldera, central Kenya Rift, Republic of Kenya: preliminary assessment of the structural characteristics of Menengai caldera and regions farther north, Nakuru, Kenya*. GDC, Kenya, unpublished report.
- Suwai, J.J., 2011: Preliminary reservoir analysis of Menengai geothermal field exploration wells. Report 32 in: *Geothermal training in Iceland 2011*. UNU-GTP, Iceland, 799-826.

## APPENDIX I: Characteristic XRD patterns for the clay minerals of well MW-19A

## 57707/MW-19A 838-840 UNT

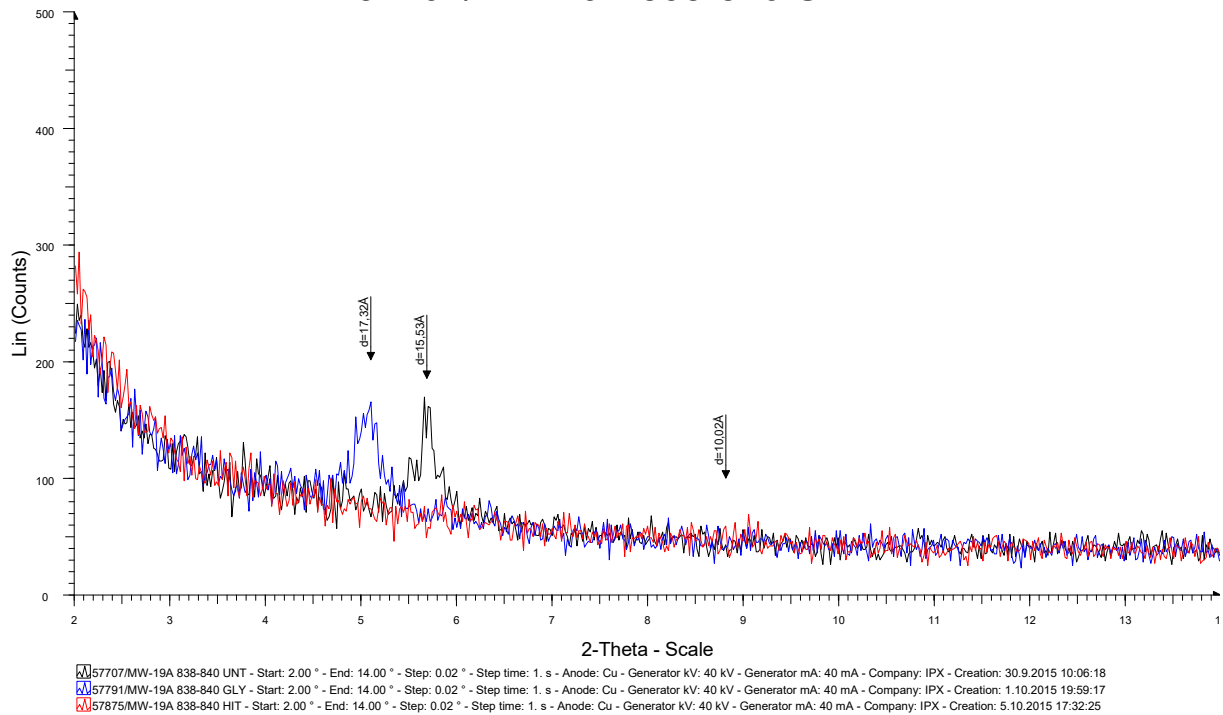


FIGURE 1: Smectite at 838-840 m depth in well MW-19A

## 57712/MW-19A 1426-1428 UNT

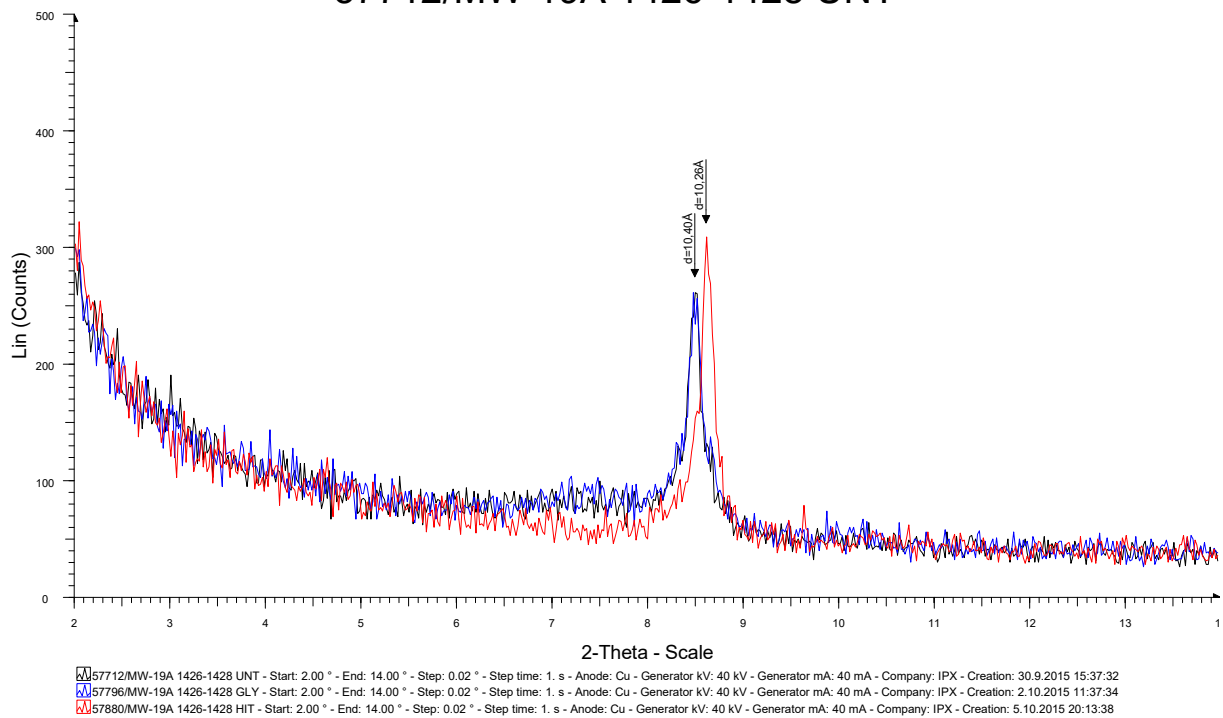


FIGURE 2: Illite at 1426-1428 m depth in well MW-19A



### 57716/MW-19A 1672-1674 UNT

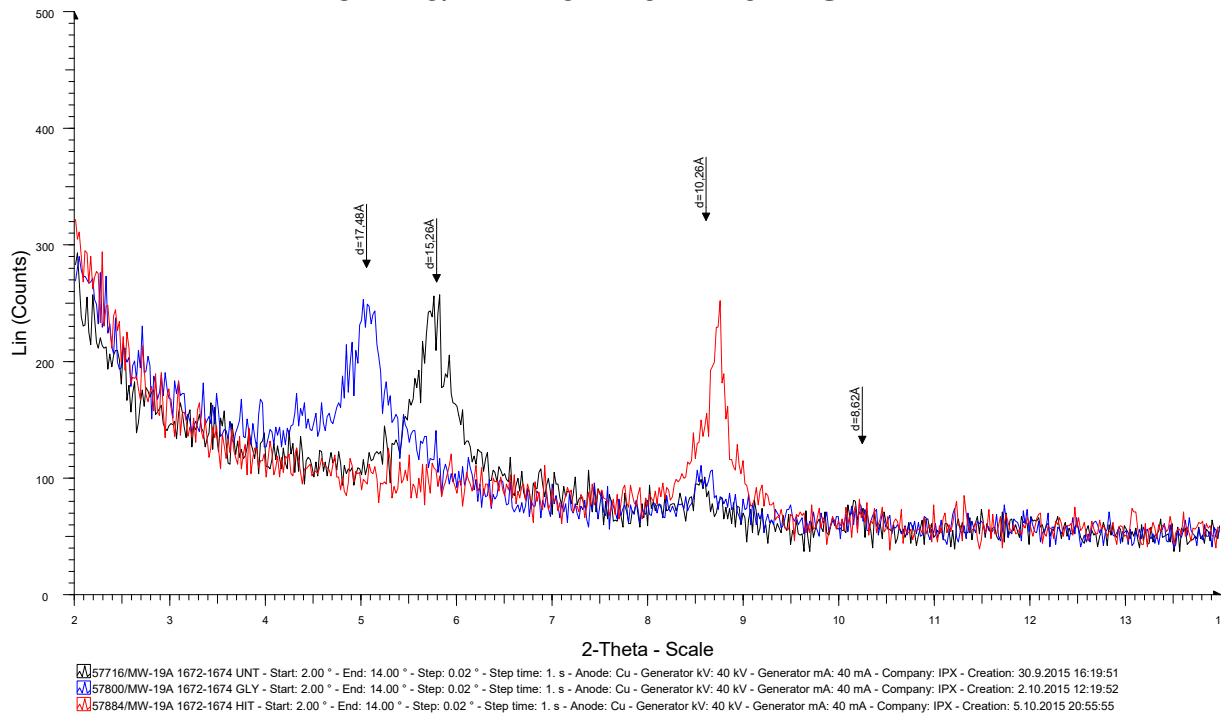


FIGURE 3: Smectite, illite and amphiboles at 1672-1674 m depth in well MW-19A

### 57721/MW-19A 1894-1896 UNT

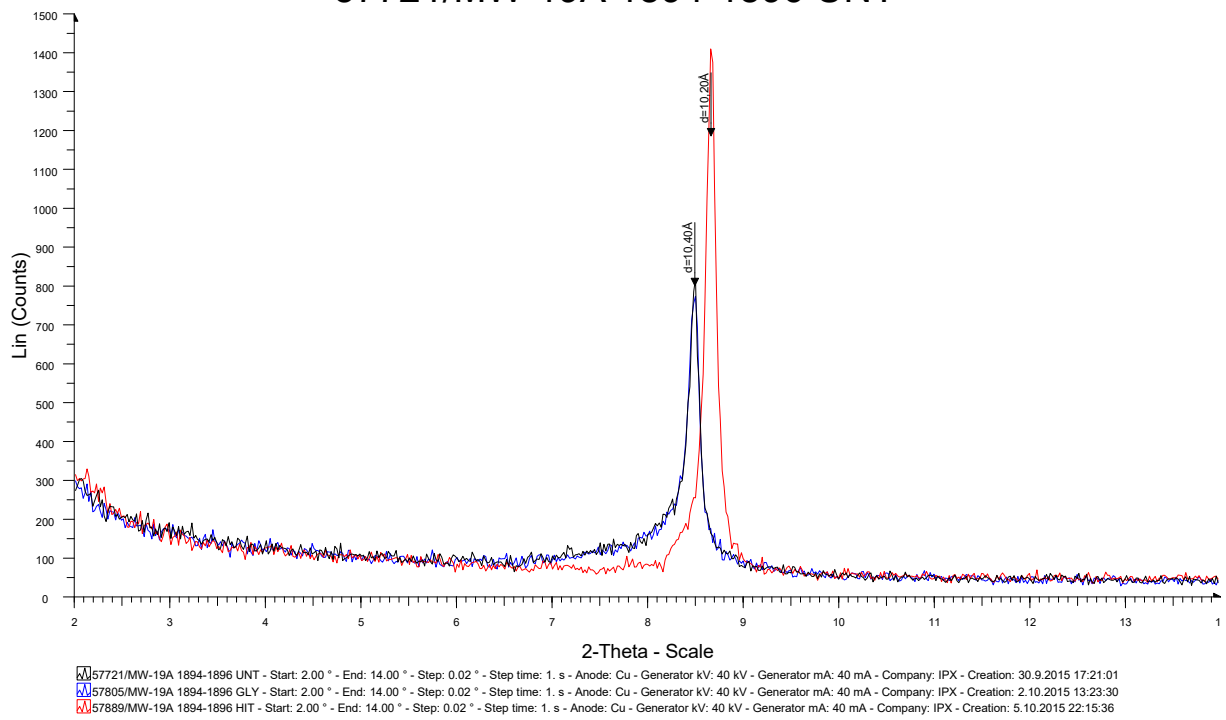


FIGURE 4: Illite at 1894-1896 m depth in well MW-19A

**APPENDIX II: Lithology of MW-19A****Post caldera volcanics**

0-6 m: *Pyroclastics*. Grey to brownish grey, loose unconsolidated deposits composed of ash and vesicular fragments of pumice lapilli particles, obsidian, glass and lithics of trachytic composition. The alteration minerals observed are oxides (opaques), some calcite and clays, indicating an interaction due to precipitation.

6-120 m: *Fine- to medium-grained trachyte*. Dark grey to greenish grey, fine-to medium-grained porphyritic rock fragments mixed with brownish grey, fine-grained vesicular rock fragments. Chalcedony is observed infilling vesicles while iron oxide is observed to precipitate at the margins and interstices of mafic minerals.

120-368 m: *Loss of returns*.

**Possible syn-caldere volcanics**

368-372 m: *Tuff*. Reddish brownish fine-grained vesicular rock mixed with dark grey fine-grained rock fragments.

372-388 m: *Fine-grained trachyte*. Dark grey fine-grained equi-granular rock mixed with reddish brown fine-grained vesicular rock fragments. Chalcedony and zeolite (scolesite) are seen infilling veins and vesicles. Iron-oxide precipitates are also evident.

388-400 m: *Tuff*. Reddish brown to grey fine-grained vesicular rock. Chalcedony and zeolite (scolesite) are seen infilling veins and vesicles. Loss of circulation at 388-390 m therefore no cuttings were recovered.

400-488 m: *Fine- to medium-grained trachyte*. Light grey to dark grey fine- to medium-grained equi-granular trachytic lava. Chalcedonic lining is observed on the rock surface and as vein fillings. The formation is moderately fractured and shows low degree of alteration. Loss of returns at 420-422, 426-428, 434-436 and 448-450 m.

488-492 m: *Loss of returns*.

**Possible pre-caldere volcanics**

492-504 m: *Tuff*. Brownish grey fine-grained vesicular rock. Scolecite and chalcedony linings are observed on the rock surfaces and also infilling vesicles.

504-508 m: *Loss of returns*.

508-544 m: *Fine-grained trachyte*. Light grey to dark grey fine-grained weakly porphyritic lava. The formation is slightly oxidized and mixed with few tuff fragments.

544-568 m: *Loss of returns*.

568-572 m: *Fine-grained trachyte* Dark grey to greenish grey fine-grained porphyritic lava. The rock shows moderate alteration to greenish clays. Sanidine phenocrysts are seen embedded in the rock matrix.

572-600 m: *Loss of returns*.

600-612 m: *Fine-grained trachyte*. Mixed cuttings composed of brownish grey fine-grained vesicular rock fragments and dark grey to greenish grey porphyritic lava.

612-638 m: *Loss of returns*.

638-796 m: *Fine-grained trachyte*. Light grey fine-grained porphyritic lava. The rock is slightly altered into greenish clays. Feldspathic fragments are also evident (640-642), this could probably be interpreted as a micro-vein. Iron oxide is observed to precipitate at the margins and interstices of mafic minerals. Intermittent returns received in this section. Loss of returns experienced at 644-658, 662-682, 684-686, 688-700, 702-722, 724-752, 766-778, and 780-796 m.

796-798 m: *Fine-grained trachyte*. Dark grey fine-grained rock formation. The rock shows medium intensity of alteration and bleaching effects. Mafic minerals are slightly altered to reddish oxides. Chlorite and abundant calcite dominate this section.

798-836 m: *Loss of returns*.

836-842 m: *Tuff*. Brownish grey fine-grained poorly crystalline vesicular rock. The rock is moderately altered into greenish clays and slightly oxidized.

842-992 m: *Fine-grained trachyte*. Mixed cuttings of brownish grey poorly crystalline rock and light grey fine-grained porphyritic rock fragments. Persistent loss of returns experienced at 842-848, 850-886 and 888-954 m; Partial returns experienced at 954-958, 992-994 m respectively. Therefore, the rock formation here cannot be defined with certainty due to the high rate of mixing.

992-1168 m: *Fine-grained trachyte*. Brownish grey moderately altered fine-grained feldspar rich lava. Phenocrysts of alkali feldspars (sanidine) and possibly quartz are seed embedded in the rock groundmass. Effects of bleaching are evident in some zones. Pyrite cubes seen disseminated on the rock surface indicative of permeability. Loss of circulation experienced at 994-1004, 1008-1054, 1064-1070, 1074-1126 and 1150-1168 m.

1168- 1326 m: *Fine- to medium-grained trachyte*. Dark grey to greenish fine- to medium-grained lava. The formation shows high intensity of alteration. Well-formed pyrite cubes are seen disseminated on the rock groundmass; it is also seen filling veins and vesicles. Quartz grains were first observed at 1202 m, but well developed crystals were noted at 1308 m forming in vesicles. Calcite is also abundant in this section. Loss of circulation at 1250-1258 m, 1316-1326 m.

1326-1418 m: *Fine-grained trachyte*. Light grey to greenish grey fine-grained porphyritic rock showing moderate to high intensity of alteration. Phenocrysts of plagioclase feldspars and pyroxenes are seen embedded in a fine groundmass. High temperature minerals characterize this formation; these include quartz, actinolite, wollastonite, chlorite and epidote. Pyrite is also seen disseminated on the rock surface. Actinolite and epidote are first seen to appear at 1418 and 1436 m respectively.

1418-1584 m: *Syenite intrusion*. Whitish grey medium- to coarse-grained porphyritic rock showing low degree of alteration. The rock also shows some mixing with slight oxidation noted between 1542 and 1584.

1584-1602 m: *Loss of returns*.

1602-1672 m: *Fine-grained trachyte*. Greenish grey to dark grey fine-grained rock showing moderate alteration. The formation shows a bleaching effect giving the rock a mottled texture. Calcite is abundant in this section. Bluish fine-grained rock fragments were observed and were handpicked for further analysis with XRD. Loss of circulation at 1668-1672 m.

1672-1674 m: *Fine-grained basalt*. Dark grey to almost black fine-grained unaltered rock.

1674-1692 m: *Loss of returns*.

1692-1734 m: *Fine-grained trachyte*. Greenish grey to whitish fine-grained porphyritic lava. The rock appears bleached exhibiting a mottled texture with abundant calcite. Pyrite is seen disseminated in the groundmass.

1734-1770 m: *Fine-grained trachyte*. Mixed cuttings composed of greenish grey to whitish fine-grained moderately altered lava with dark grey to black fine-grained rock fragments. Epidote colouration is observable starting at 1750 m and is seen to persist with depth.

1770-1802 m: *Fine-grained basalt*. Dark grey to black fine-grained hypocrySTALLINE rock. Between 1778 and 1780 the rock appears finer. Calcite and pyrite specs characterize this section.

1802-1920 m: *Fine-grained trachyte*. Greenish grey to whitish fine-grained feldspar rich rock. The formation shows high intensity of alteration with abundant calcite and exhibiting a mottled texture. At 1844-1846 the formation is slightly oxidized.

1920-1952 m: *Syenite*. Light grey fine- to medium-grained lava showing low to medium degree of alteration. Loss of circulation experienced 1924-126, 1928-1930 and 1946-1952.

1954-2008 m: *Fine-grained trachyte*. Brownish to greenish grey fine-grained lava. The rock is fractured and shows effects of bleaching into whitish clays. The rock exhibits low intensity of alteration and has abundant calcite. Major loss zones encountered at 1954-1956, 1960-1962, 1966-1972, 1974-1986, 1988-1992 and 1994-2004 m.

2008-2354 m: *Loss of returns*.